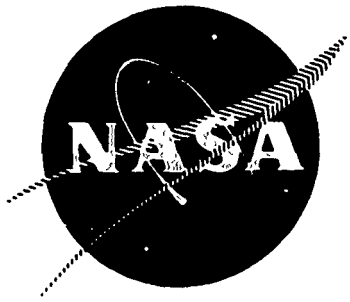

NASA CR-134479

DROPLET BREAKUP IN ACCELERATING GAS FLOWS
PART II: SECONDARY ATOMIZATION

by

L. J. Zajac

ROCKETDYNE
A DIVISION OF ROCKWELL INTERNATIONAL
6633 CANOGA AVENUE, CANOGA PARK, CALIFORNIA

prepared for
NATIONAL AERONAUTICS AND SPACE ADMINISTRATION

NASA-Lewis Research Center
NAS3-14371

NOTICE

This report was prepared as an account of Government-sponsored work. Neither the United States, nor the National Aeronautics and Space Administration (NASA), nor any person acting on behalf of NASA:

A. Makes any warranty of representation, expressed or implied, with respect to the accuracy, completeness, or usefullness of the information contained in this report, or that the use of any information, apparatus, method, or process disclosed in this report may not infringe privately-owned rights; or

B. Assumes any liabilities with respect to the use of, or for damages resulting from the use of, any information, apparatus, method or process disclosed in this report.

As used above, "person acting on behalf of NASA" includes any employee or contractor of NASA, or employee of such contractor, to the extent that such employee or contractor of NASA or employee of such contractor prepares, disseminates, or provides access to any information pursuant to his employment or contract with NASA, or his employment with such contractor.

Requests for copies of this report should be referred to

National Aeronautics and Space Administration
Scientific and Technical Information Facility
P.O. Box 33
College Park, Md. 20740

1. Report No.	2. Government Accession No.	3. Recipient's Catalog No.
NASA CR-134479		

4. Title and Subtitle	5. Report Date
DROPLET BREAKUP IN ACCELERATING GAS FLOWS PART II: SECONDARY ATOMIZATION	October 1973 6. Performing Organization Code

7. Author(s)	8. Performing Organization Report No.
L. J. Zajac	R-9337-2
	10. Work Unit No.

9. Performing Organization Name and Address	11. Contract or Grant No.
Rocketdyne Division, Rockwell International Canoga Park, California, 91304	NAS3-14371
	13. Type of Report and Period Covered Contractor Report

12. Sponsoring Agency Name and Address	14. Sponsoring Agency Code
National Aeronautics and Space Administration Washington, D.C., 20546	

15. Supplementary Notes

Technical Manager, R. J. Priem, NASA-Lewis Research Center, Cleveland, Ohio

16. Abstract

An experimental investigation to determine the effects of an accelerating gas flow on the atomization characteristics of liquid sprays was conducted. The sprays were produced by impinging two liquid jets. The liquid was molten wax (Shell 270) and the gas was nitrogen. The use of molten wax allowed for a quantitative measure of the resulting dropsize distribution. The study was conducted in two parts. In one part, the effects of the gas on the spray after the spray was formed were examined. The results of this study, reported herein, indicate that a significant amount of droplet breakup will occur as a result of the action of the gas on the liquid droplets. Empirical correlations are presented in terms of parameters that were found to affect the mass median dropsize most significantly, e.g., the orifice diameter, the liquid injection velocity, and the maximum gas velocity. An empirical correlation for the normalized dropsize distribution is also presented. These correlations are in a form that may be incorporated readily into existing combustion model computer codes for the purpose of calculating rocket engine combustion performance.

The other part of the study dealt with the effects of the accelerating gas flow on the initial, or primary, spray atomization. The results obtained in that portion of the program are presented in a companion volume entitled, "Droplet Breakup in Accelerating Gas Flows, Part I: Primary Atomization" (R-9337-1).

17. Key Words (Suggested by Author(s))	18. Distribution Statement
Droplet Breakup Primary Atomization Secondary Atomization Liquid Sprays Cold Flow Simulation Accelerating Gas Flows	

19. Security Classif. (of this report)	20. Security Classif. (of this page)	21. No. of Pages	22. Price*
Unclassified	Unclassified	70	

* For sale by the National Technical Information Service, Springfield, Virginia 22151

Page Intentionally Left Blank

FOREWORD

The work described herein was conducted by Rocketdyne, a Division of Rockwell International, in accordance with the terms of Contract NAS3-14371 for the National Aeronautics and Space Administration, Lewis Research Center, Cleveland, Ohio. Dr. R. J. Priem of the Lewis Research Center Served as the NASA Technical Manager. The Rocketdyne Program Manager was Mr. L. P. Combs. Technical guidance of the program was provided by Dr. D. T. Campbell. This report is presented in two volumes:

NASA CR-134478--Part I: Primary Atomization
(Rocketdyne internal report R-9337-1)

- NASA CR-134479--Part II: Secondary Atomization
(Rocketdyne internal report R-9337-2)

Page Intentionally Left Blank

CONTENTS

Page Intentionally Left Blank

ILLUSTRATIONS

TABLES

Page Intentionally Left Blank

NOMENCLATURE

A_c = cross-sectional area of gas flowfield

C_p = drag coefficient

d = orifice diameter

D = droplet diameter

$\overline{D}$ = mass median dropsize

$\overline{D}_c$ = mass median dropsize when $V_{g_M} = V_L$

$\overline{D}_o$ = mass median dropsize when $V_g = 0$

$\overline{D}_2$ = mass median dropsize produced by secondary atomization process

F = drag force

F_∞ = drag force for infinitely spaced droplets

L = gas acceleration ramp length

L_p = distance from injector to diffuser or gas acceleration ramp

Re = Reynolds number

S = droplet spacing

T_g = gas temperature

T_L = liquid temperature

V_o = drop velocity

V_g = gas velocity

V_{g_o} = initial gas velocity

V_{g_M} = maximum gas velocity

V_L = liquid gas velocity

$\dot{w}$ = mass flowrate

$\dot{w}_g$ = gas flowrate

$\dot{w}_L$ = liquid flowrate

X = axial distance or droplet spacing

α = flowrate ratio, $\dot{w}_L/\dot{w}_g$, or drag ratio, F/F_∞

δ = separation ratio, X/D

ΔV = gas-to-liquid relative velocity, $V_{g_M} - V_L$

ρ_g = gas density

ρ_L = liquid density

1.0 SUMMARY

This report contains the results of an experimental cold-flow study of the effects of an accelerating gaseous flowfield on the atomization of a liquid spray. The objective was to quantify the influence on droplet breakup of several geometric and dynamic parameters of the liquid spray and gas flowfield; specifically, the injector orifice diameter and injection velocity, the liquid-to-gas mass flux ratio, the length over which the gas underwent acceleration, and the change in the gas velocity over this length. The ranges of these parameters used in the tests corresponded with typical rocket engine combustion conditions. Like-doublet, impinging-jet injector elements were used exclusively. Molten was was employed as the liquid, and the gas was heated, ambient pressure nitrogen.

The results of this study have demonstrated that a substantial amount of secondary atomization may be sustained after a spray has been formed as a result of accelerating the combustion gas which carries the droplets. Reductions in the mass median dropsize by a factor of 2 or more were observed at even moderate gas velocities (less than, for example, 200 ft/sec). The parametric changes that contributed most to the amount of secondary atomization were changes in the maximum gas velocity, V_{g_M}, and in the liquid orifice diameter, d, and injection velocity, V_L.

Empirical correlations, in terms of these three parameters, which provide good agreement with the measured mass median dropsizes, $\overline{D}_2$, were found to be*:

$$\overline{D}_2 = \overline{D}_c \left[1 - 1.77\text{x}10^{-3}\, \overline{D}_c \, \frac{\Delta V}{V_L} \quad \exp\left(-0.24 \, \frac{\Delta V}{V_L} \left| \frac{\Delta V}{V_L} \right| \right) \right]$$

over the range $-1 \leq \frac{\Delta V}{V_L} \leq 1.25$ and

$$\overline{D}_2 = \overline{D}_c \left[1 - 1.52\text{x}10^{-3}\, \overline{D}_c \right] \quad -12 \, \ell n \left(\frac{\Delta V}{V_L} \right)$$

for $\frac{\Delta V}{V_L} > 1.25$

where

$$\frac{\Delta V}{V_L} = \frac{V_{g_M} - V_L}{V_L}$$

and

$$\overline{D}_c = 2.2\text{x}10^4 \, d^{0.375} / V_L^{0.75}$$

*d in inches, V_L and V_g in ft/sec, $\overline{D}_2$ and $\overline{D}_c$ in microns

As with most empirical formulations, the above equations should not be used outside their range of applicability. In this case, the above formulations should be used only when $140 \leq \overline{D}_c \leq 360\mu$ which covers the range of orifice diameters and liquid velocities examined. The rate of acceleration should be limited to a range of from 2.5 to 400 ft/sec-in., with a maximum gas velocity of 1000 ft/sec. Even with these limits, the correlations should cover most rocket engine conditions.

The fact that the gas is accelerating is not explicity included in the correlations. However, its effect was implicit in the data used to obtain the correlations in that the liquid droplets were also accelerated. Thus, the measured dropsizes reflect the effects of the actual gas-to-droplet velocity difference, even though the liquid injection velocity is used in the correlations.

The length over which the spray was exposed to the accelerating gas flow found to have a small effect on the resulting dropsize and is, therefore, not included in the correlation. No effect of the spray density, i.e., the liquid-to-gas mass flux ratio, was observed.

The dropsize distributions were also examined as part of this study. Without exception, the distributions tended to become more nearly monodisperse as the gas velocity was increased. No single distribution function could be found which would fit all of the data; however, the Rosin-Rammler normalized distribution function given by:

$$\frac{d(\dot{w}/\dot{w}_{TOT})}{d(D/\overline{D})} = \frac{2.46\ (D/\overline{D})^{1.46}}{(1.21)^{2.46}}\ \exp\left[-\frac{(D/\overline{D})^{2.46}}{1.61}\right]$$

agreed quite well with the experimental data and, in particular, with the large dropsize portion of the distribution. In the above, $\dot{w}/\dot{w}_{TOT}$ is the cumulative mass fraction of drops having diameter smaller than D, and $\overline{D}$ is the mass median dropsize.

2.0 INTRODUCTION

Combustion in liquid propellant rocket engines is frequently vaporization-rate limited. As a consequence, calculated droplet vaporization rates are used as the foundation of the analytical combustion models which provide combustion efficiencies and axial gas velocity profiles (Ref. 1 and 2). Generally, the results obtained from these analytical tools are in good agreement with expermental observations. However, with relatively large propellant dropsizes and/or low chamber contraction ratios, the combustion models frequently underpredict combustion efficiencies(Ref. 3). This is thought to be the result of the influence of the combustion gas velocity on atomization, an effect which is, at present, not incorporated at all in most existing combustion models.

Although adequate quantitative definitions of droplet size under rocket engine conditions have not been made, present technology has been used as a qualitative guide for design of chamber geometries to improve combustion performance. One such study was conducted wherein the effect of contraction ratio on performance was evaluated for the propellant combination of OF_2/B_2H_6 (Ref. 4). The analytically determined performance trends were verified by hot-firing tests. The magnitude of the c* performance increase (about 11 percent) was correctly forecast by the combustion model using combustion gas velocity changes caused by contraction ratio changes. The success of these efforts indicates the significance of the combustion gas velocity as a factor in propellant spray atomization.

The combustion chamber gas velocity can influence atomization of the liquid propellants in two distinct ways: (1) by gas/liquid shear on the jets, sheets, and ligaments, the gas velocity can affect the initial spray formation, (i.e., primary atomization); and (2) after this initial period of spray formation, the gas can cause further atomization by acting on and shattering the droplets in the liquid spray (secondary atomization). Both of these atomization processes have been studied, in some degree, by previous investigators (Ref. 5 through 8). However, these studies have dealt primarily with single droplets and/or a constant velocity gas flow. To the author's knowledge, no data existed to describe atomization when a liquid spray is exposed to an accelerating gas, a condition which more closely approximates the environment of the combustion chamber.

To fill this technical gap, a cold-flow experimental study was initiated to (1) delineate, from among several gas and liquid parameters, those which contribute more significantly to droplet breakup, and (2) quantitatively evaluate the extent of droplet breakup caused by changes in these parameters. The combustion chamber parameters that were experimentally simulated in this study were the combustion gas velocity profile, chamber length, spray density, injector orifice diameters, and injection velocity. Both the primary and secondary atomization processes were examined. Contained herein are the results of the secondary atomization study. A companion report (Ref. 9) contains the results of the study of primary atomization in an accelerating flowfield.

Page Intentionally Left Blank

3.0 EXPERIMENTAL APPARATUS

DESCRIPTION OF TEST APPARATUS

The apparatus used to perform the experiments, shown schematically in Fig. 1, consisted of two basic components: a test section and a subsonic diffuser. A photograph of the apparatus is presented in Fig. 2.

Basically, the test section was a 10- by 10-inch cross section by 43-inch long "box" which housed the two-phase flow during the atomization process. Gaseous nitrogen was brought into the test section at the far upstream end, passed through a porous plate "flow straightener," flowed axially through the test section, and exhausted through the subsonic diffuser. Liquid wax was brought into the test section through a cylindrical tube located along the axis of the test section. Liquid was injected to flow axially with the gas through a like-doublet element located on the downstream end of the tube. The tube was moveable, which enabled the injector to be positioned at any location between the downstream end of the test section and a point 32 inches upstream.

To maintain the wax in a molten state, the supply tube and the injector were jacketed and heated by a 240 F oil flow. The nitrogen was also heated to a temperature above the melting point of the wax (>140 F) to prevent the possibility of wax solidification within the test section.

Acceleration of the two-phase flow was achieved by means of ramps bolted to the sides of the test section. Four pair of ramps, having axial lengths of 2, 4, 8, and 16 inches, were utilized. The height of all of the ramps was 4 inches, thus providing a 5 to 1 contraction ratio (10- by 10-inch to 10- by 2-inch cross section). Test section area variation through the flow acceleration zone was linear with axial distance. A photograph showing the 2-inch-long ramps mounted in the test section is presented in Fig. 3. The injector element is also visible in the photo. The ramps can be removed from the test section for constant gas velocity tests.

The second basic component of the test apparatus was the subsonic diffuser. The purpose of the diffuser was to rapidly and efficiently reduce the gas velocity, and hence the droplet drag forces, to prevent (or at least to minimize) any additional atomization downstream of the test section.

A vacuum system was installed at the inlet to the diffuser (Fig. 1) to exhaust the boundary layer and prevent the buildup of an adverse pressure gradient that could cause separation. With the vacuum system activated, the gas velocity profile within the diffuser was measured and found to agree with one-dimensional gas dynamic theory, as shown in Fig. 4, for all gas flowrates used in the experiments. Without the boundary layer suction, diffuser stall (i.e., flow separation) occurred at the 8 lb/sec flowrate. To prevent this situation from occurring during an atomization test, the boundary layer suction was employed in all experiments.

A cold-gas injection system was also installed near the inlet to the diffuser. The intent was to mix cold (≈20 F) GN_2 with the hot (≈150 F) two-phase mixture to reduce the bulk temperature of the gas and hasten solidification of the wax.

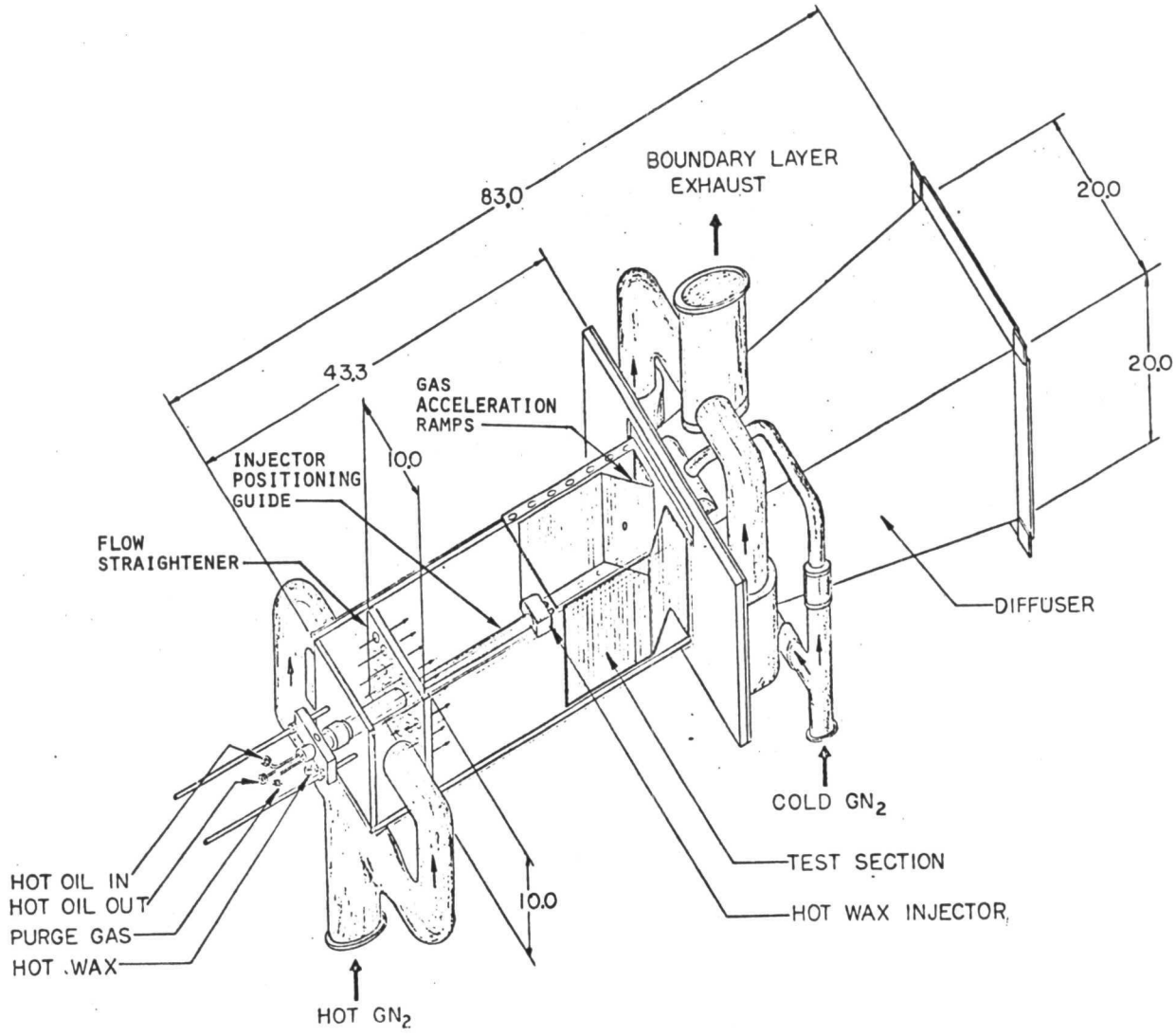

Figure 1. Schematic Illustration of Test Section

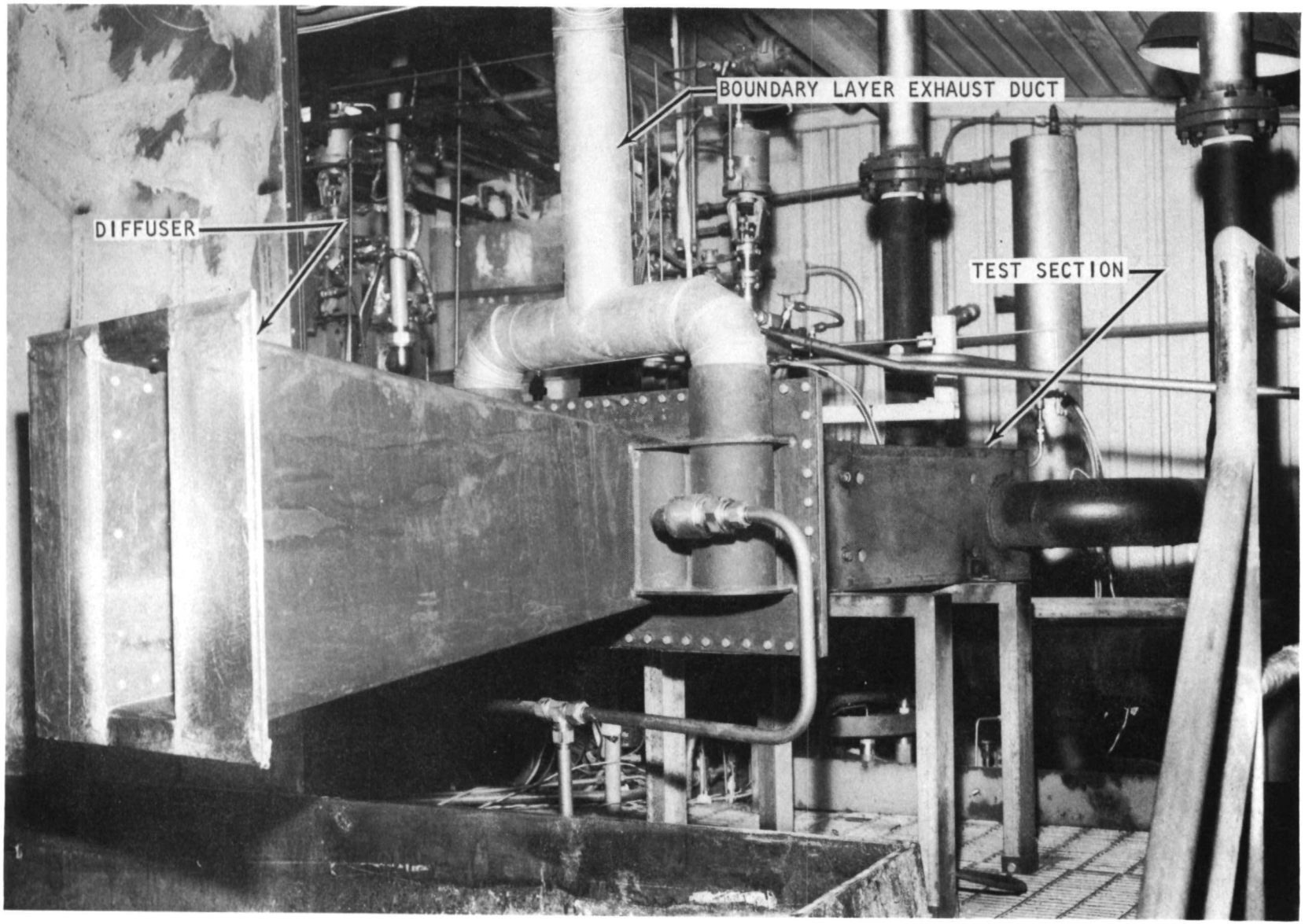

5AA34-7/20/72-S1A

Figure 2. Experimental Apparatus

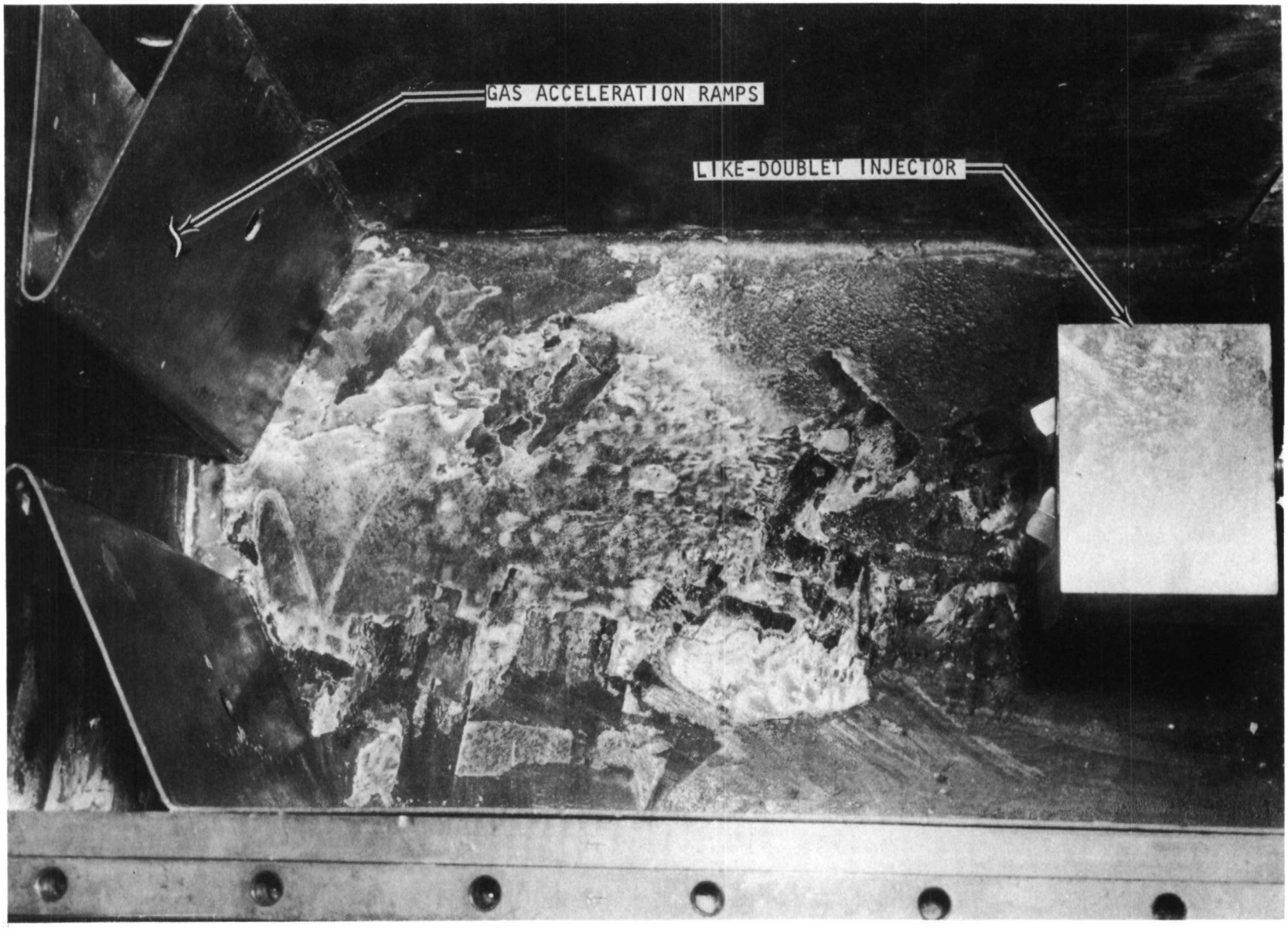

5AA34-7/20/72-S1E

Figure 3. Interior of Test Section

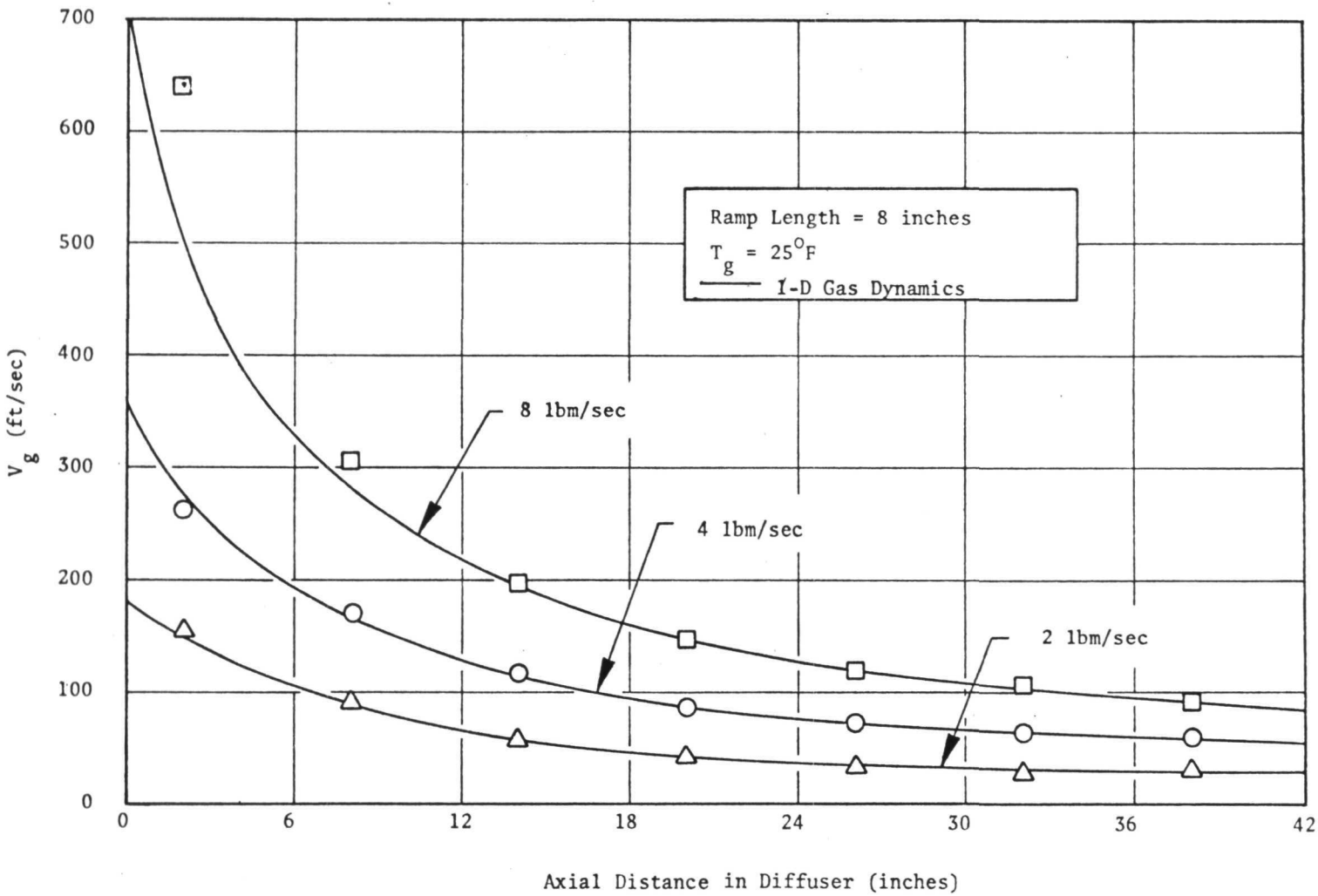

Figure 4. Gas Velocity Profile in Subsonic Diffuser

It was found, in the checkout tests, that this procedure had no effect on the measured dropsizes. However, it was beneficial in that it helped to reduce accumulation of wax on the diffuser walls and, therefore, its use was continued.

After deceleration in the diffuser, the two-phase flow was exhausted into the atmosphere just above an 18- by 50-foot collection table, as shown in Fig. 5. An overhead water spray was directed downward to force the wax droplets toward the table. The table was also water flushed to prevent the wax from adhering to the collection table. The wax particles were washed from the table into a catch basin where they were scooped from the surface of the water and placed in a plastic bag for storage until a sample could be taken for analysis.

INJECTOR CHARACTERISTICS

A total of 5 like-doublet injectors was used in the program. These injectors had orifice diameters ranging from 0.055 to 0.162 inches and length-to-diameter ratios of about 8. The inlets to the orifices were rounded to a radius of 1.5 diameters. The injector ensemble actually consisted of three pieces, 2 externally threaded orifice plugs, and a 2- by 4- by 3-inch long manifold block which was common to all injector assemblies. The injector assembly is shown in Fig. 6. The distance from the orifice exit to the impingement point was 5 orifice diameters with an included angle of 60 degrees for all injector assemblies.

To assess the effects of the gas flow on the atomization process, the "characteristic" dropsize, $\overline{D}_o$, of the injector was first determined. It is defined as the dropsize produced by the injector, at a given liquid velocity, in a static environment, i.e., no gas flow. This dropsize can be determined from the empirical relation (Ref. 10):

$$\overline{D}_o = 15.9 \times 10^4 \, d^{0.58}/V_L \qquad (1)$$

where d is the orifice diameter (in inches) and V_L the injection velocity (in ft/sec).

A series of tests was performed to verify that this function would correctly predict the mass median dropsize. The results of these tests for three of the injectors are shown in Table I. As shown there, the measured and calculated dropsizes agree quite well. The remaining two injectors, having 0.073- and 0.124-inch diameters, were not checked but they should behave in accordance with Eq. 1.

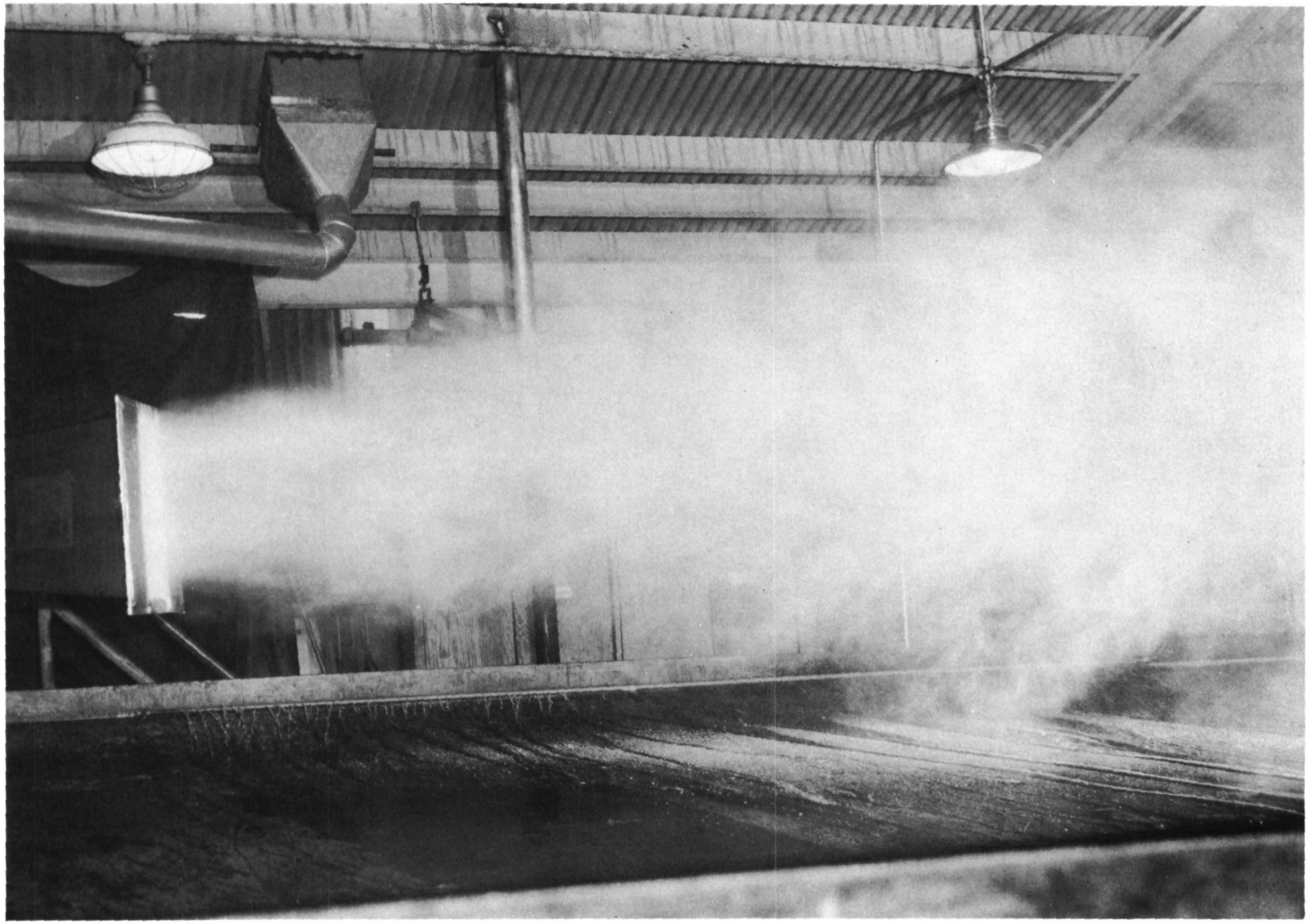

5AA34-7/20/72-S1B

Figure 5. Wax Droplet Collection Table

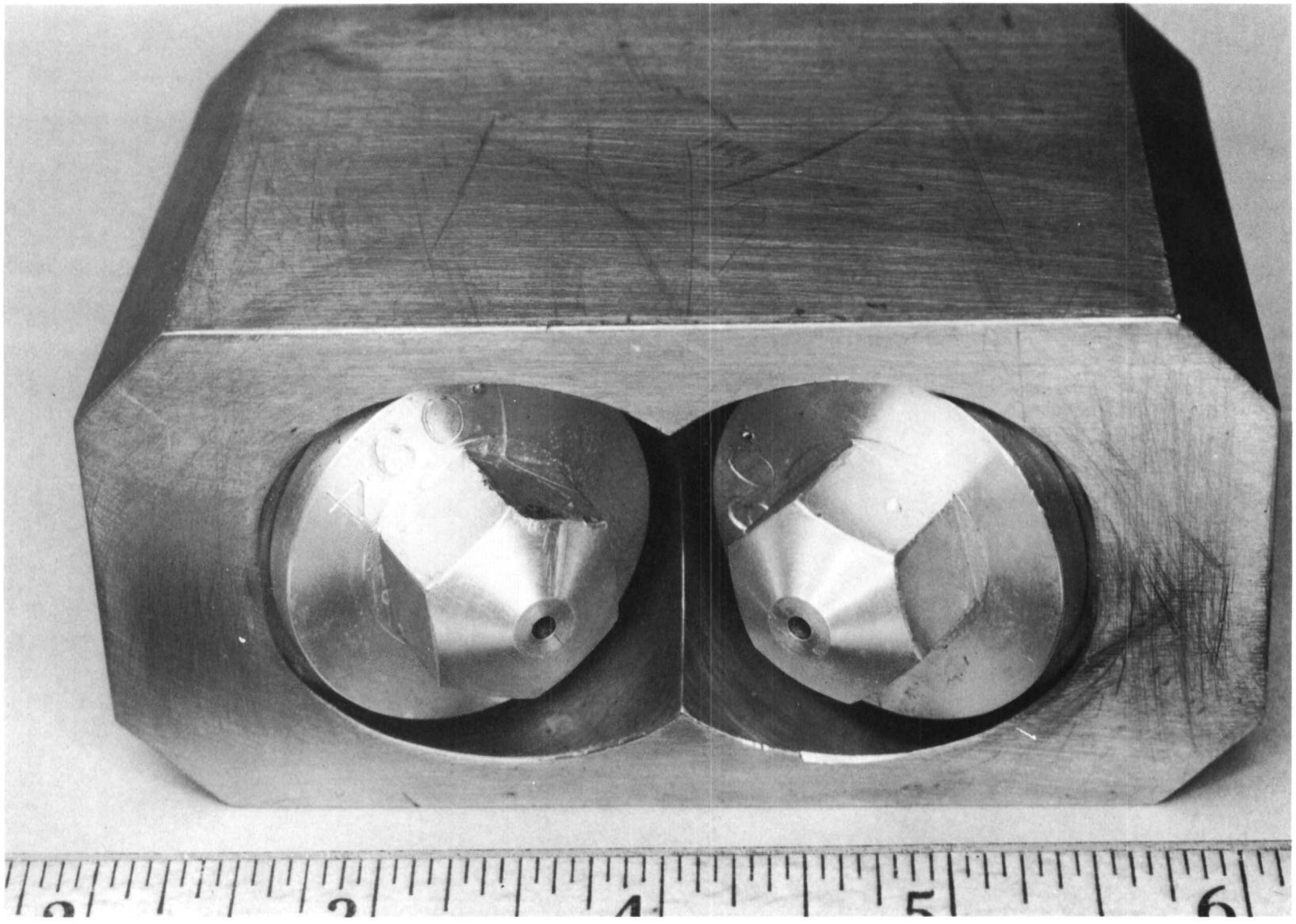

5AD34-8/10/73-S1B

Figure 6. Typical Like-Doublet Injector Used in Atomization Study

TABLE I. SUMMARY OF INJECTOR CHECKOUT TESTS

d, inch	V_L, ft/sec	$\overline{D}_o$ (μ) Measured	$\overline{D}_o$ (μ) Calculated
0.055	80	332	349
	120	240	254
	160	190	191
	200	150	152
0.094	44	555	530
	109	365	374
	142	290	292
	195	197	209
	250	167	163
	295	135	139
0.162	95	575	590
	145	405	387
	165	315	340

Page Intentionally Left Blank

4.0 EXPERIMENTAL TECHNIQUE

The experimental technique employed in this study was to inject molten wax in a gaseous flowfield and then, by collecting the spray, to determine, through a sieving process, the dropsize distribution and, from this, the mass median dropsize. This sieving technique and the method of evaluating the mean dropsize are discussed in Appendix A. Prior to the initiation of the main experimental effort, a series of checkout experiments was performed to delineate the effects of this technique on the experimental results.

Since the wax was injected into a confined area, some impingement of wax droplets on the walls of the test section was unavoidable. To be certain that the results were unaffected by this wax/wall impingement, several tests were performed in which the degree of potential spray impingement on the wall was varied by changing the axial position of the injector. The test conditions and results of two of these tests, labeled C1 and C2, are shown in Table II. The distance, L_p, corresponds to the distance measured from the injector to the inlet of the diffuser (see insert in Table II). Posttest measurements of the wax attached to the walls indicated that about 10 percent of the total amount of wax injected impinged with the wall when L_p was 10.5 inches, as compared to 30 percent when L_p was 32.5 inches. However, this produced a very small difference in the mass median dropsize, as shown in Table II. In addition, very similar dropsize distributions were obtained, as shown in Fig. 7. Since the 30-percent figure exceeded the amount of wax/wall impingement sustained in the subsequent atomization tests, it was concluded that confining the spray within the test section would not significantly affect the results.

At high gas velocities, boundary layer suction was necessary to prevent a stall condition within the diffuser. It was conceivable that the smaller droplets in the spray could be exhausted with the gas removed from the diffuser. However, examination of the boundary layer exhaust ducting revealed only minimal wax deposits. Furthermore, an examination of the median dropsizes obtained both with and without boundary layer exhaust revealed no change as can be seen by comparing the results of tests C-5 and C-3 shown in Table II. It was concluded, therefore, that this part of the experimental technique also had no effect on the results.

To enhance droplet solidification downstream of the test section, cold gas was injected into the diffuser. If the median dropsize were found to increase as a result of this process, it would imply that additional atomization was occurring in the diffuser and that it was prevented by rapidly freezing the droplets. However, tests conducted both with and without cold-gas injection revealed that this process had little effect on the measured median dropsize. This is seen from a comparison of the results of test C-4 (Table II), where no gas was injected, and test C-3, where 1 lb/sec of 20 F gas was injected into a 2 lb/sec effluent from the test section. It was noted however, that the cold-gas injection did reduce wax accumulation on the walls. Hence, it was retained for this latter purpose.

TABLE II. SUMMARY OF FACILITY CHECKOUT TESTS

Run No.	L_p, inch	V_g, ft/sec	T_g, F	$\dot{W}_g$, lb/sec	$\dot{W}_D$, lb/sec	Boundary Layer Suction	$\overline{D}$, microns	Comments
C-1	10.5	51	152	2.09	0	No	306	Effect of L_p
C-2	32.5	43	115	2.04	0	No	318	(±2 percent)
C-3	15.5	45	135	2.04	1.0	Yes	320	Effect of boundary layer suction
C-5	15.5	45	125	2.04	1.0	No	318	(<1 percent)
C-4	15.5	44	125	2.04	0	Yes	318	Effect of $\dot{W}_{Dif}$
C-3	15.5	45	135	2.04	1.0	Yes	320	(<1 percent)

NOTE: V_L = 109 ft/sec

d = 0.094 inch

$\dot{W}_L$ = 0.5 lb/sec

T_L = 200 F

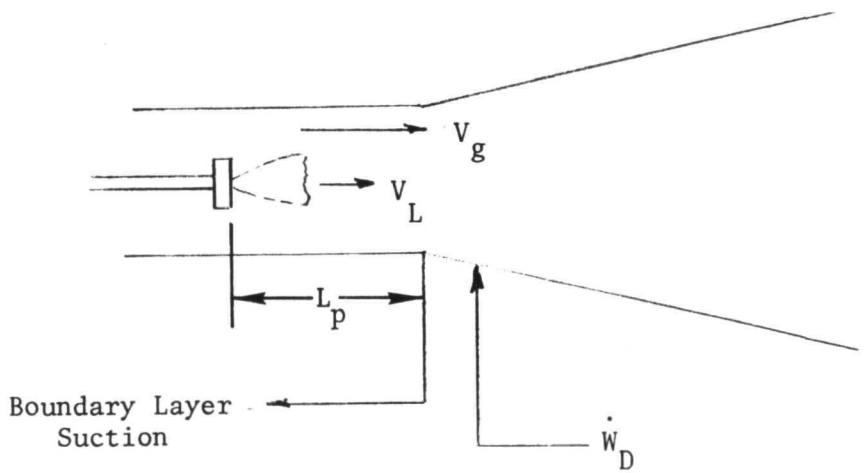

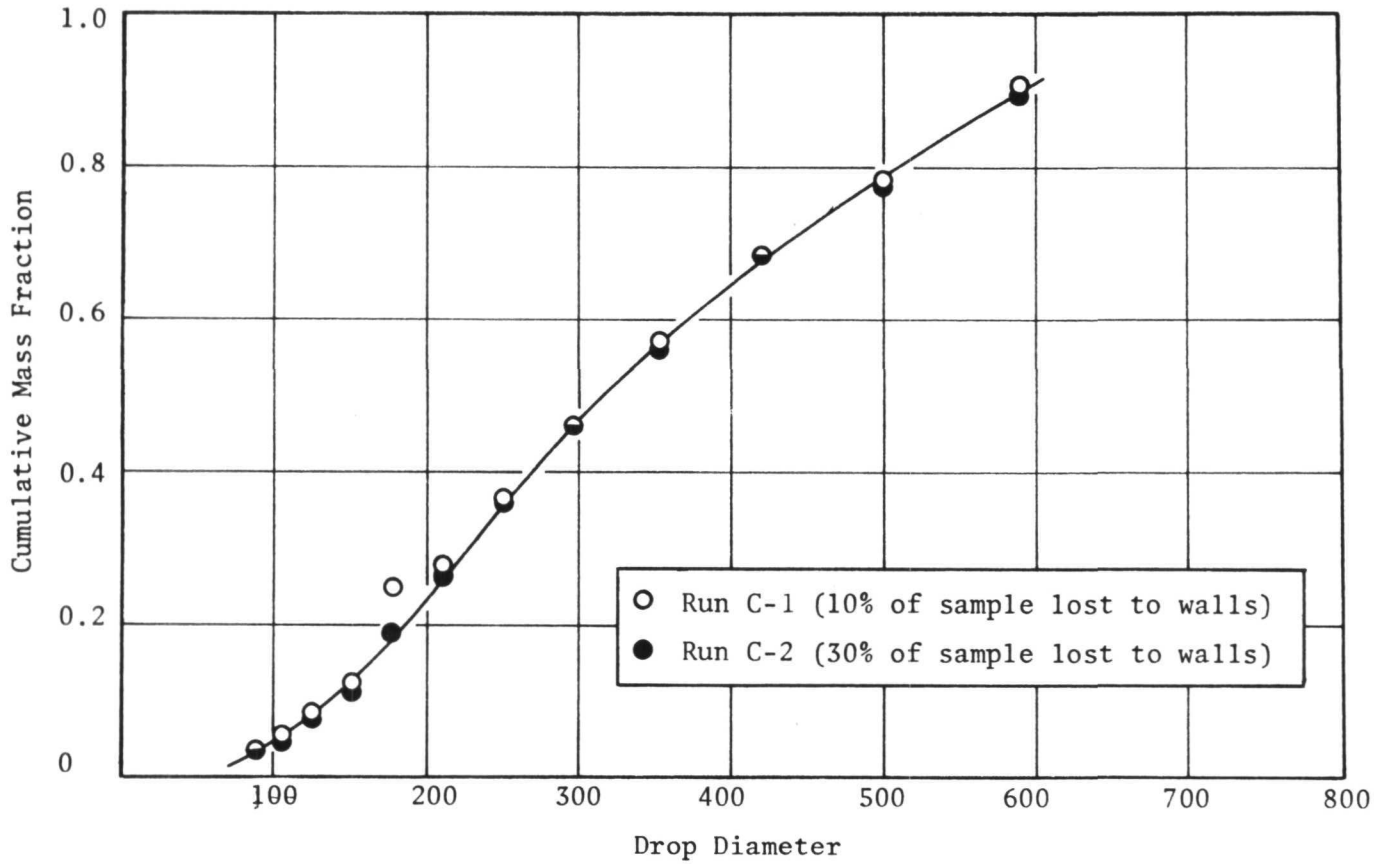

Figure 7. Comparison of Dropsize Distributions Obtained in Checkout Tests

The question of where the atomization was occurring was a serious one that would affect the conclusions drawn from this study. It was possible that any secondary atomization observed could have occurred either prior to the acceleration section or downstream of it in the diffuser. To ensure that the bulk of the secondary atomization was not occurring upstream of the accelerating section, several tests were performed under similar liquid injection conditions. In one test, No. C-5 in Table III, the gas flow was zero, and a median dropsize of 365 microns, which agreed with Eq. 1, was measured. Then the gas velocity was increased to 41 ft/sec and held constant, i.e., with the ramps removed. This produced a median dropsize of 335 microns (run C-6 in Table III), indicating that some atomization was occurring because of the gas flow. Finally, with the ramps installed, a gas flow that yielded a velocity of about 48 ft/sec in the constant area section and a maximum velocity of 247 ft/sec was established. In this test, the injector was located 10.5 inches upstream of the beginning of the ramp. (as can be seen from Table II, this distance should be sufficient for completion of the primary atomization, i.e., for the spray reach an equilibrium dropsize; longer distances produced no change in the mean dropsize.) The mass median dropsize obtained in this test was 140 microns (run C-7). Since the gas velocity in the spray formation region was the same as in run C-6, the median dropsize at the start of convergence should also be about 335 microns. It is, therefore, evident that acceleration of the gas from 48 to 247 ft/sec produced a change in the dropsize from about 335 to 140 microns. Thus, the bulk of the secondary atomization occurred downstream of the ramp inlet.

A second test (run No. C-8 in Table III), conducted under identical gas and liquid conditions as run C-7, yielded a median dropsize of 174 microns. These two runs, plus additional repeat tests throughout the program, established an experimental error band of ±12 percent on the mass median dropsize for this experimental technique.

TABLE III. SUMMARY OF CHECKOUT TESTS

Run No.	V_{g_o}, ft/sec	V_{g_M}, ft/sec	$\overline{D}$, microns
C-5	0	0	365
C-6	41	41	335
C-7	48	247	140
C-8	48	247	174
C-9	222	222	155

V_L = 109 ft/sec
d = 0.094 inch
$\dot{W}_L$ = 0.5 lb/sec
T_L 200 F

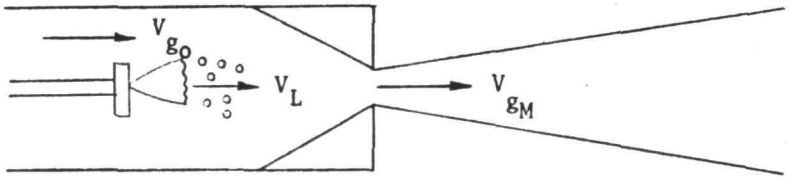

However, it could not be clearly established that atomization was not occurring in the diffuser. Therefore, the results may be exhibiting the effects of some atomization in the diffuser, although the indications are that this is not the case. For example, as shown by run No. C-9 of Table III, a test conducted at a constant gas velocity of 222 ft/sec yielded a mass median dropsize similar to those obtained when the maximum gas velocity, under accelerating flow conditions, was 247 ft/sec. This could happen only if droplet breakup occurred within very small spatial intervals since the maximum gas velocity is attained only briefly at the throat of the test section when accelerating ramps are used.

Page Intentionally Left Blank

5.0 EXPERIMENTAL RESULTS

The experimental study was designed to determine independently the influences of several injector and gas flow parameters on the atomization of liquid sprays. The parameters that were examined and the ranges over which they were varied are listed in Table IV.

TABLE IV. RANGE OF EXPERIMENTAL PARAMETERS

Length of Acceleration Zone, inches	2, 4, 8, 16				
Gas $\Delta\dot{V}$ ($V_{g_{max}} - V_{g_o}$), ft/sec	40, 100, 150, 200, 400, 800				
Orifice Diameter, inch	0.055	0.073	0.094	0.124	0.162
Liquid Velocity, ft/sec	76, 160	45, 90, 180	54, 109, 200	122, 244	95, 145
Liquid-to-Gas Mass Flux Ratio	0.016, 0.032, 0.064, 0.125, 0.25, 0.33, 0.50, 1.0, 1.25				

A total of 94 tests was conducted, of which 25 were with constant gas velocities through the test section. The test conditions and measured mass median dropsizes are listed in Tables V (constant gas velocity tests) and VI (accelerating flow tests).

Both the mass median dropsizes and the dropsize distributions were examined as part of this study. The effects of the various design and flow parameters on these two characteristic spray parameters are presented separately in the following paragraphs.

MASS MEDIAN DROPSIZE RESULTS

Influence of Distance

The effect of the distance over which the spray was exposed to the accelerating gas is shown in Fig. 8. These data were obtained with the 0.094-inch orifice diameter element at a liquid velocity of 109 ft/sec, but are typical of the results obtained with other elements and/or injection velocities. The various symbols in the figure represent different gas velocities.

Although there is a consistent trend of decreasing dropsize with increased ramp length, the total change in the median dropsize between L = 2 and L = 16 inches is small, on the order of 10 percent for all gas and liquid velocities examined. Since this percentage change corresponds roughly to the accuracy of the experimental technique, it was not possible to determine whether the change was real or simply data scatter. In eigher case, the effect of length on the secondary atomization process can be neglected.

TABLE V. SUMMARY OF CONSTANT GAS VELOCITY TESTS

d, inch	V_L, ft/sec	$\dot{W}_L$, lb/sec	$\dot{W}_L/\dot{W}_g$	V_g, ft/sec	T_L, F	T_g, F	ρ_g, lb/ft^3	$\overline{D}_o$, microns	$\overline{D}_2$, microns
0.094	109	0.50	0.060	222	194	230	0.053	374	155
			0.105	117	194	158	0.059		255
			0.245	47	200	150	0.060		287
			0.062	187	205	170	0.058		197
			0.085	112	210	23	0.075		280
			0.330	41	235	225	0.053		335
			0.500	27	235	225	0.053		340
	200	0.92	0.450	58	220	275	0.059	204	230
	200	0.92	0.172	118	220	157	0.058	204	200
	200	0.92	0.114	190	220	165	0.058	204	170
0.055	76	0.125	0.062	49	210	150	0.059	348	365
	76	0.125	0.015	220	215	230	0.053	248	148
	152	0.250	0.125	48	220	148	0.060	191	226
	152	0.250	0.050	120	220	160	0.069	191	200
	152	0.250	0.031	220	223	220	0.053	191	150
0.073	90	0.250	0.125	50	215	155	0.059	373	350
	90	0.250	0.031	220	220	265	0.050	373	152
	180	0.500	0.244	44	225	135	0.061	199	216
	180	0.500	0.062	195	225	235	0.052	199	156
0.124	122	1.00	0.500	44	225	125	0.062	395	315
	122	1.00	0.125	220	225	225	0.053	395	190
	244	2.00	0.125	117	225	250	0.051	198	210
	244	2.00	0.250	233	225	270	0.050	198	155
0.162	145	2.00	1.00	48	235	148	0.060	387	325
0.162	145	2.00	0.250	220	235	225	0.053	387	193

TABLE VI. SUMMARY OF VARIABLE GAS VELOCITY TESTS

d, inch	V_L, ft/sec	$\dot{W}_L$, lb/sec	W_L/W_g	V_{g_o}, ft/sec	V_{g_M}, ft/sec	$V_{g_M}-V_L$, ft/sec	T_L, F	T_g, F	ρ_g, lb/ft^3	L, inch	$\bar{D}_o$, microns	$\bar{D}_2$, microns
0.094	109	0.500	1.25	11	55	-54	230	220	0.052	2	374	345
			1.25	10	50	-59	220	170	0.058	8		318
			1.25	10	50	-59	225	220	0.052	16		310
			0.50	28	140	31	238	225	0.031	2		243
			0.050	25	125	16	220	170	0.058	8		250
			0.50	28	140	31	225	224	0.051	16		208
			0.33	42	213	104	230	238	0.051	2		197
			0.33	37	177	68	225	170	0.058	8		215
			0.33	42	213	104	225	240	0.051	16		185
			0.25	50	238	129	225	125	0.058	2		132
			0.25	48	247	138	208	153	0.060	8		140
			0.25	48	247	138	230	165	0.060	8		174
			0.25	46	234	125	220	120	0.063	16		150
			0.25	46	234	125	215	120	0.063	16		152
			0.125	90	485	376	225	142	0.065	4		135
			0.125	95	515	406	220	195	0.061	8		128
			0.063	148	1013	904	222	255	0.079	2	373	148
			0.063	145	991	882	220	240	0.080	4		150
			0.063	141	950	841	220	205	0.083	8		140
			0.063	150	1038	929	220	275	0.078	16		135
			0.063	150	1038	929	220	275	0.078	16		115
0.073	90	0.25	0.125	51	248	158	220	145	0.056	2		160
			0.125	47	240	150	218	135	0.061	4		149
			0.063	93	485	395	220	163	0.063	2		119
				90	487	397	215	160	0.065	4		162
				92	500	410	220	175	0.063	8		130
				91	495	405	220	170	0.063	8		155
				89	481	391	215	150	0.066	16		135
0.124	122	1.0	0.50	47	240	118	203	135	0.061	4	395	188
			0.50	49	252	130	200	165	0.059	8		160
			0.25	90	490	368	220	163	0.065	4		135
			0.25	97	526	404	220	210	0.060	16		162
			0.125	147	1000	878	225	245	0.079	4		152
0.162	145	2.0	1.0	52	250	105	235	150	0.055	8	387	235
			1.0	52	250	105	235	150	0.055	16		205
			0.5	93	480	335	235	150	0.063	2		140
			0.25	147	1000	855	225	240	0.055	8		130
			0.25	147	1000	855	235	240	0.079	16		170

TABLE VI. (Concluded)

d, inch	V_L, ft/sec	$\dot{W}_L$, lb/sec	W_L/W_g	V_{g_o}, ft/sec	V_{g_M}, ft/sec	$V_{g_M}-V_L$, ft/sec	T_L, F	T_g, F	ρ_g, lb/ft^3	L, inch	$\bar{D}_o$, microns	$\bar{D}_2$, microns
0.094	200	1.0	0.500	50	235	35	235	125	0.058	2	204	150
			0.500	48	248	48	215	155	0.060	8		142
			0.250	90	485	285	215	155	0.065	4		130
			0.250	84	454	254	215	115	0.069	16		113
			0.125	142	925	725	230	195	0.082	2		118
			0.125	145	987	787	205	235	0.080	4		100
			1.00	28	140	-60	205	145	0.060	4		192
0.055	160	0.25	0.125	51	245	85	220	135	0.056	2	191	122
0.055	160	0.25	0.125	54	275	116	220	215	0.053	2	191	135
0.073	180	0.50	0.250	51	245	65	224	144	0.056	2	199	150
			0.250	56	281	108	215	255	0.051	8		130
			0.125	93	480	300	220	163	0.063	2		145
			0.125	91	496	316	215	170	0.064	8		107
			0.063	148	1013	833	225	255	0.079	2		104
			0.063	144	975	795	200	225	0.081	4		95
0.124	244	2.0	0.50	91	492	248	210	165	0.079	8	198	116
			0.250	149	1025	781	225	265	0.078	2		125
			0.250	146	994	750	203	240	0.080	4		120
			0.250	147	1000	754	215	245	0.079	8		116
			0.250	153	1063	817	205	295	0.076	16		122
0.094	54	0.250	0.250	25	125	71	220	127	0.053	2	632	300
			0.125	46	234	180	215	123	0.054	2		150
			0.062	95	520	466	220	142	0.065	2		140
			0.032	143	950	896	230	200	0.082	2		115
0.073	45	0.125	0.062	51	245	200	210	137	0.056	2	627	150
0.073	45	0.125	0.015	146	980	935	212	225	0.080	2	627	121
0.162	95	1.15	1.15	28	140	45	235	155	0.055	8	593	235
0.162	95	1.15	0.57	55	280	185	230	225	0.052	2	593	149
0.162	95	1.15	0.14	131	850	755	230	125	0.089	2	593	123

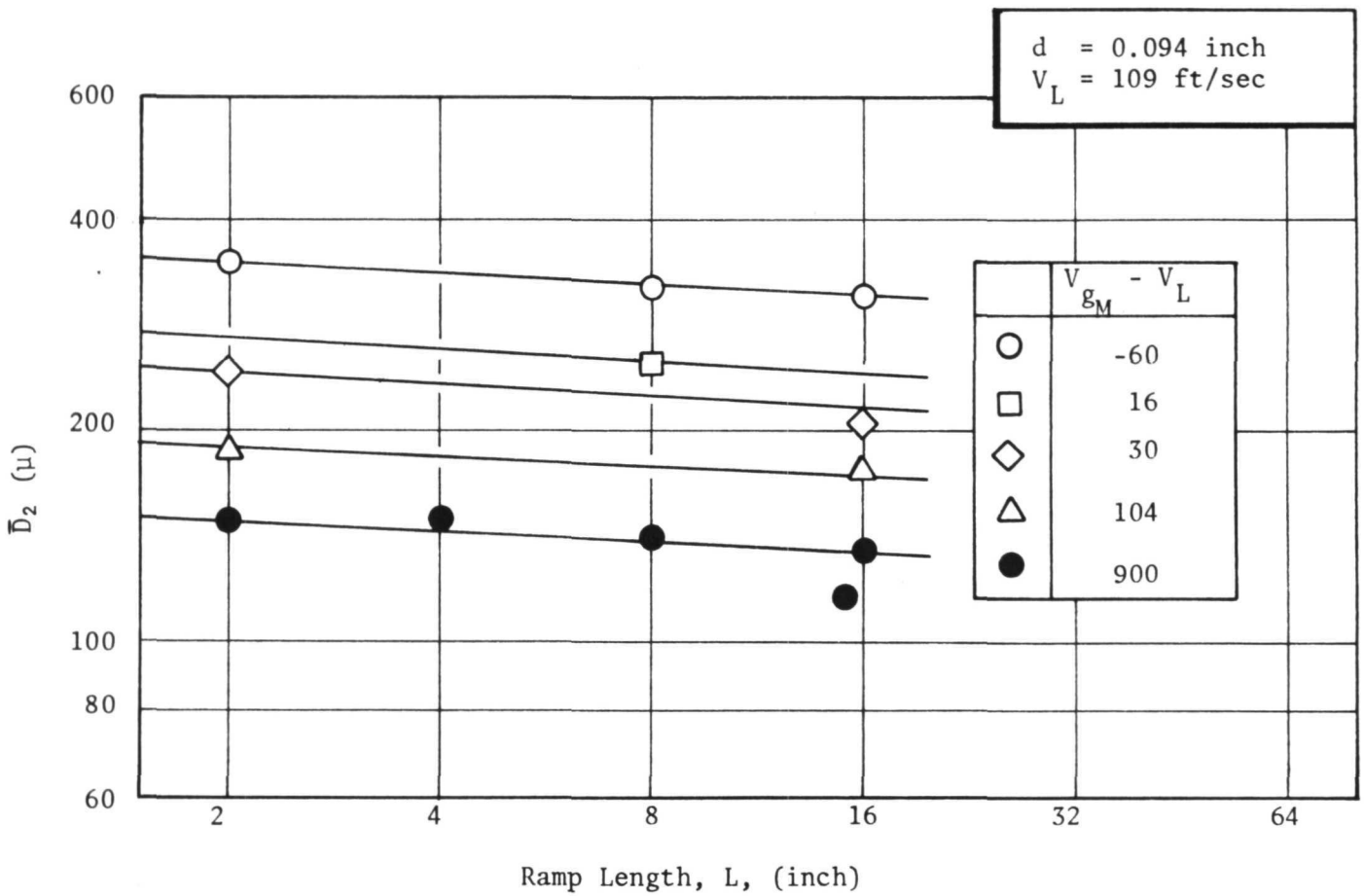

Figure 8. Effect of Distance on the Mass Median Dropsize

Influence of Gas Velocity

The effect of the gas velocity on the mass median dropsize is shown in Fig. 9. For clarity, the data shown are only those obtained with the 0.094-inch-diameter element at an injection velocity of 109 ft/sec. However, the behavior of $\overline{D}_2$ illustrated by Fig. 9 is characteristic of that observed with all injector orifice diameter/liquid velocity combinations examined. The results obtained with both accelerating and constant velocity gas flows are shown in the figure.

The abscissa in Fig. 9 is the nondimensional velocity $(V_{g_M} - V_L)/V_L$ where V_{g_M} is the maximum gas velocity in the test section, and V_L is the liquid injection velocity. This function was suggested by Yeo (Ref. 11) as a correlating parameter (for the mean dropsize obtained when spray fans were inserted into a constant gas flow), and was found to be the best parameter for correlating the results of this study. Consequently, the remainder of the results are presented in terms of this function. It should be noted, however, that in Fig. 9, V_L is constant. Therefore, the variation of $\overline{D}$ shown there is a result of gas velocity changes only.

As shown in Fig. 9, a substantial decrease in the mass median dropsize is obtained as the gas velocity is increased. As a point of reference, the dropsize obtained at these injector conditions, but at zero gas velocity ($\Delta V/V_L$ = -1 in Fig. 9), is about 374 microns (from Eq. 1). In this example, at a gas velocity of about 200 ft/sec ($\Delta V/V_L \simeq 2$) a 60-percent decrease (from 365 to 150 microns) in the median dropsize was measured. In typical rocket engine combustion chambers, the gas velocities usually are substantially higher than 200 ft/sec.* Therefore, neglecting this effect could seriously impact a combustion performance calculation.

The results shown in Fig. 9 are typical of the data obtained with other injector diameters and liquid velocities in that most of the droplet breakup could be accomplished by maximum gas velocities less than about twice the liquid velocity, i.e., $\Delta V/V_L \lesssim 2$. Above this value the dropsize was found to be a slowly varying function of the gas velocity suggesting the possibility of a limiting dropsize. This result, which is discussed further in a later section, is believed to be a twofold effect of: (1) the gas drag on the particles which accelerate the droplets and tends to decrease the realizable value of the relative gas-to-droplet velocity, and (2) the fact that increasingly greater gas-to-droplet relative velocities are required to break up the smaller median dropsize spray generated as secondary atomization proceeds.

The data shown in Fig. 9 also indicate that essentially the same median dropsize was obtained in the constant gas velocity experiments and in the accelerating flow tests if the maximum gas velocity was the same in the two tests.

As an example, for a propellant combination with a c of 5000 ft/sec, a chamber velocity of 200 ft/sec would be exceeded for any contraction ratio is less than 12.

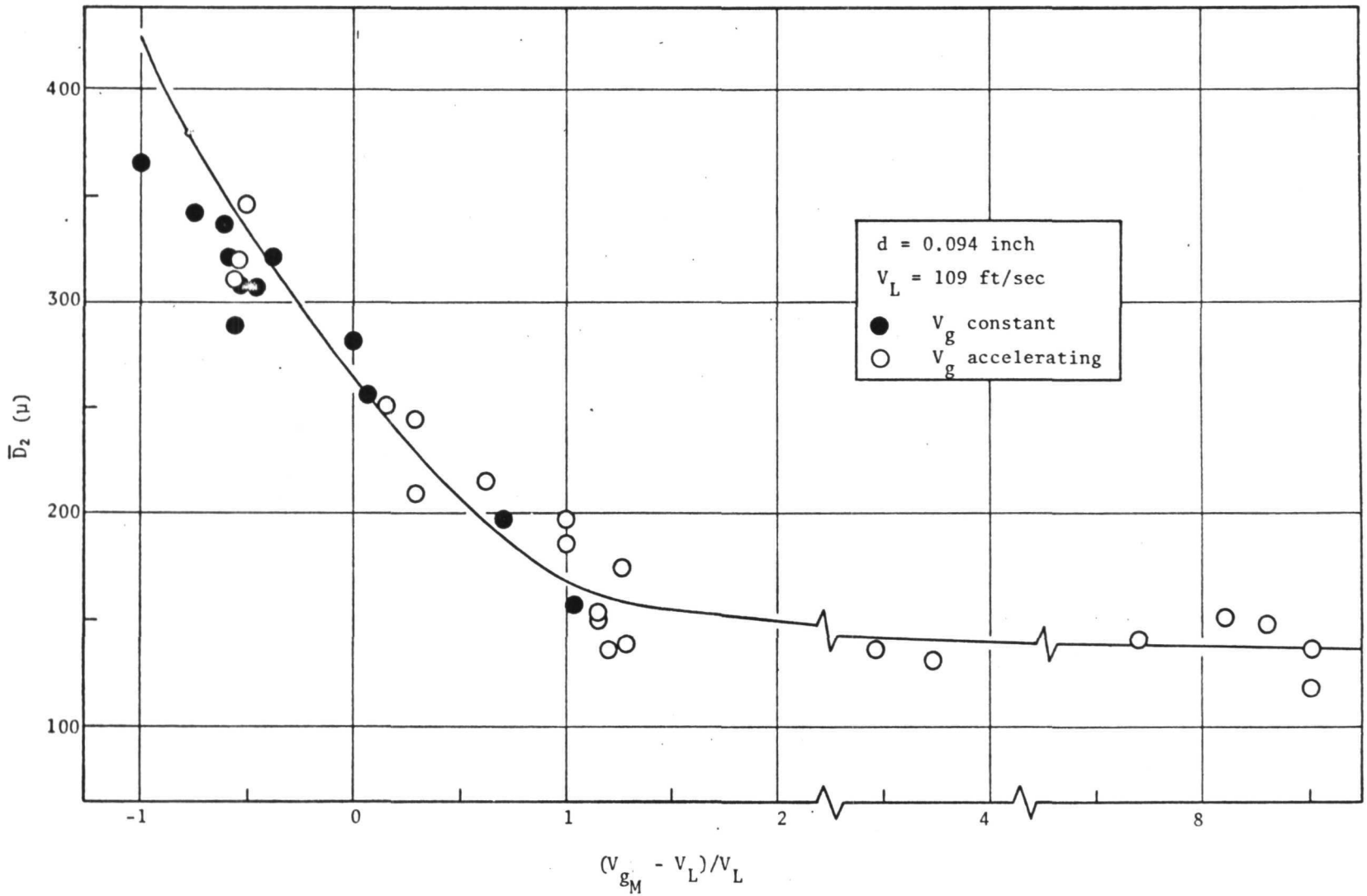

Figure 9. Influence of Gas Velocity on Mass Median Dropsize; $\bar{D}_o$ = 374 Microns

Since, in the accelerating flow tests, the maximum velocity is attained at the test section throat for only a very short time duration, the above result can be achieved only if the breakup time of the droplets is very small. This conclusion is consistent with the fact that the length of the gas acceleration ramps (or, equivalently, the residence time of the droplets in this zone) had a negligible effect on the median dropsize.

Influence of Orifice Diameter and Injection Velocity

These two injector parameters were not varied independently. Rather, orifice diameters that were typical of rocket engine doublet-type injectors were selected and the injection velocities were chosen to yield nominal mass median dropsizes, $\overline{D}_o$, of either 200, 400, or 600 microns under static gas conditions (i.e., $V_g = 0$). The values of $\overline{D}_o$ selected were considered to be typical of rocket propellant $\overline{D}$'s. These parameters are related by the empirical function (Ref. 10):

$$\overline{D}_o = 15.9 \times 10^4 \, d^{0.57}/V_L \qquad (1)$$

which was verified during the experimental checkout of the injectors used in this study (see Table I). The significance of this median dropsize is that it is related to the mass median dropsize of the spray just before it enters the gas acceleration section, and thus represents an "initial" dropsize.

The constant velocity and accelerating gas flow data obtained with combinations of d and V_L yielding nominal $\overline{D}_o$ values of 400, 200, and 600 microns are presented in Fig. 10 through 12, respectively. Once again, the median dropsize is plotted as a function of the parameter $(V_{g_M} - V_L)/V_L$.

In Fig. 10, the solid line represents the 0.094-inch orifice diameter data of Fig. 9. It can be seen from Fig. 10 that the data obtained with the various orifice diameter/injection velocity combinations, all of which correspond to a $\overline{D}_o$ value of about 400 microns, agree quite well with the d = 0.094 inch and V_L = 109 ft/sec data for which $\overline{D}_o$ = 374 microns.

Similar results were obtained with combinations of d and V_L that yielded $\overline{D}_o$'s of about 200 microns, as shown in Fig. 11, and 600 microns as shown in Fig. 12. Thus, for constant values of $\Delta V/V_L$, the effect of variations in the injector parameters can be assessed in terms of the characteristic dropsize, $\overline{D}_o$.

As can be inferred from Fig. 11 and 12, the secondary dropsize, $\overline{D}_2$, appears to vary monotonically with $\overline{D}_o$. For example, when $\overline{D}_o$ is decreased from 400 to 200 microns, a corresponding decrease in $\overline{D}_2$ is observed for all values of $\Delta V/V_L$, as shown in Fig. 11. Similarly, when $\overline{D}_o$ is increased, the secondary dropsize increases. However, for values of $\overline{D}_o > 400$ microns, the influence of $\overline{D}_o$ appears to be negligible when $\Delta V/V_L \gtrsim 1$, as shown in Fig. 12.

Influence of the Liquid-to-Gas Mass Flux Ratio

The final parameter investigated in this study was the liquid-to-gas mass flux ratio, α. It is defined simply as the ratio of the flowrates, and represents

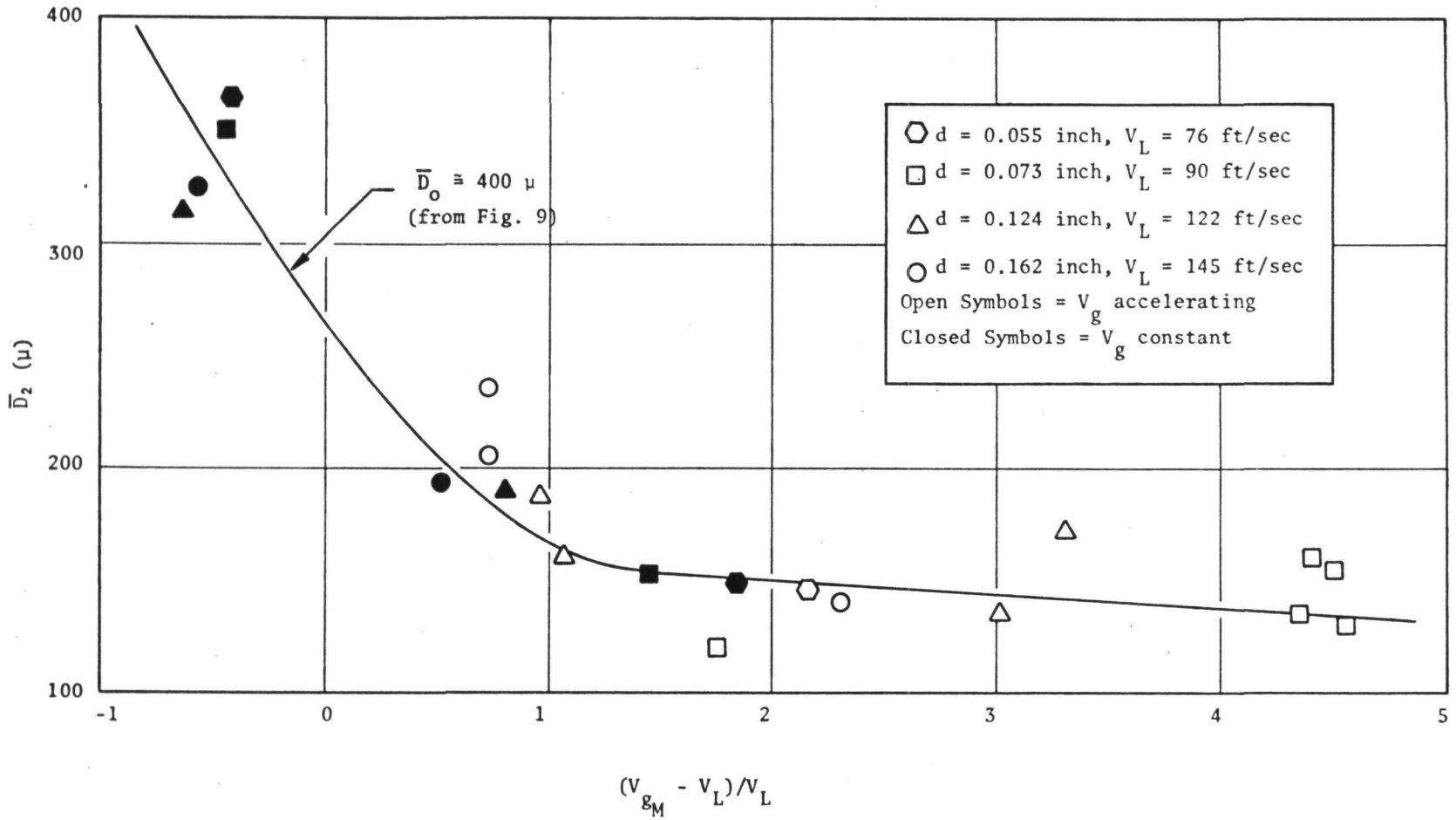

Figure 10. Variation of Mass Median Dropsize With $\Delta V/V_L$; $\overline{D}_o \simeq 400$ Microns

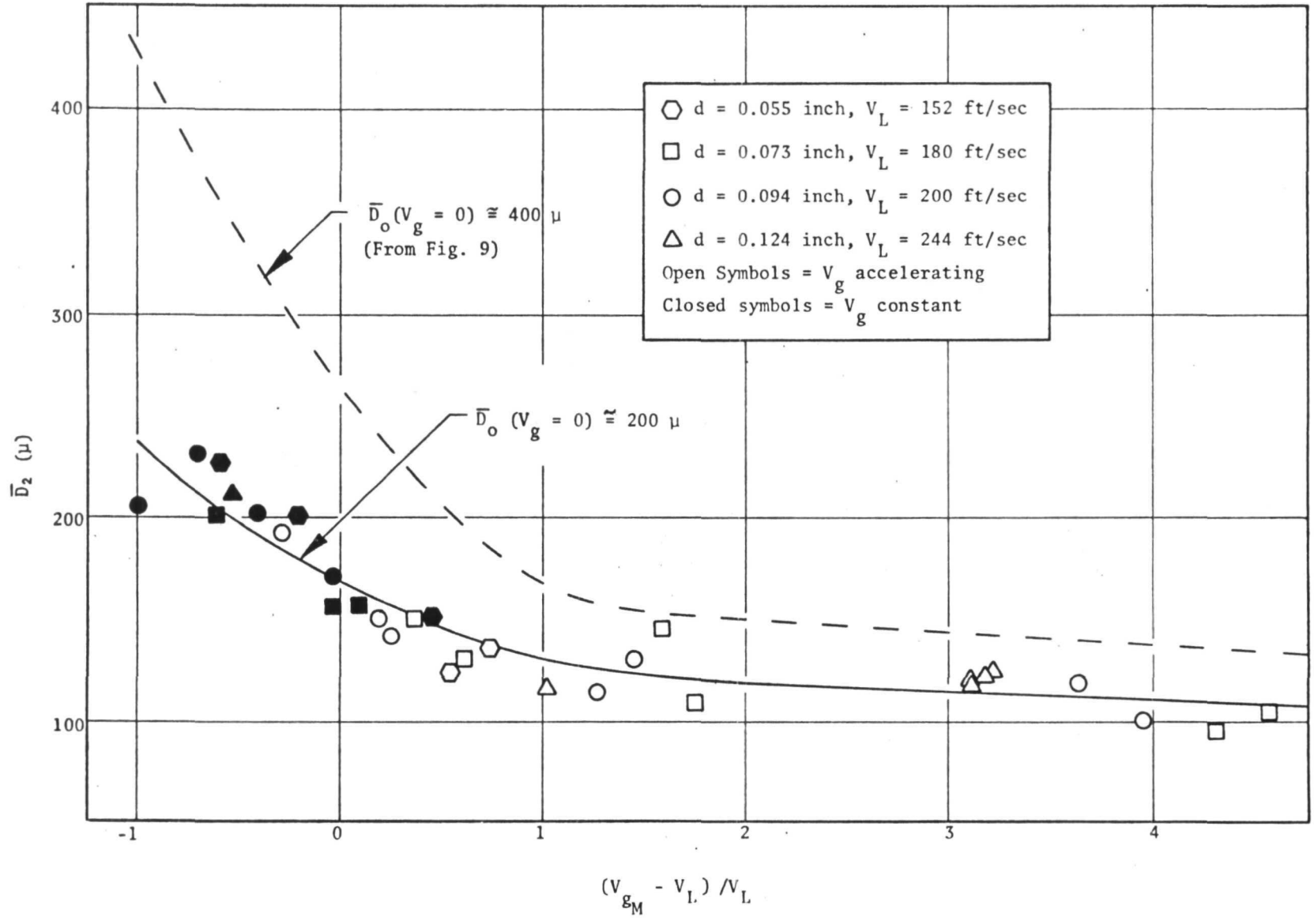

Figure 11. Variation of Mass Median Dropsize With $\Delta V/V_L$; $\bar{D}_o \simeq 200$ Microns

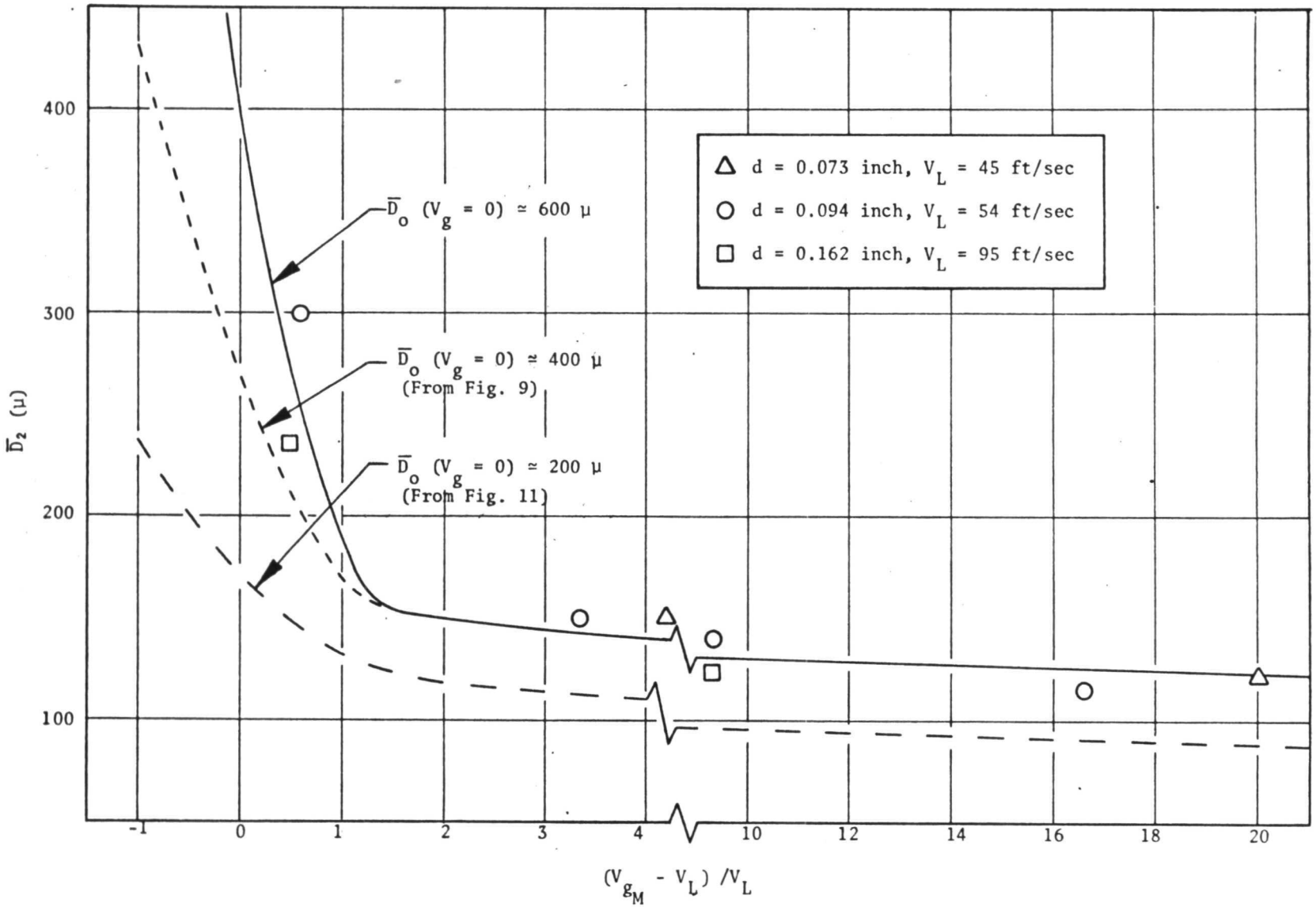

Figure 12. Variation of Mass Median Dropsize With $\Delta V/V_L$; $\bar{D}_o$ = 600 Microns

an average liquid particle loading in a plane normal to the test section. This parameter was varied independently of both the gas velocity and $\overline{D}_o$.*

Shown in Fig. 13 are the mass median dropsizes obtained at various values of α. The data obtained at two nominal values of $\Delta V/V_L$ of 1.5 and 3.5 and a $\overline{D}_o$ of 400 microns are shown. Although α was varied over an 8:1 range, no effect on the mass median dropsize was observed. A similar result was obtained when the characteristic dropsize of the spray, $\overline{D}_o$, was 200 microns as shown in Fig. 14.

For the data shown in Fig. 13 and 14, $\Delta V/V_L$ varied somewhat about the nominal values. However, as can be seen from Fig. 10 and 11, the variation of $\overline{D}_2$ is small over the range of $\Delta V/V_L$ in question. For example, in Fig. 13, $\Delta V/V_L$ varied from 1 to 2 for the data shown while from Fig. 10, $\overline{D}_2$ changes from about 160 to 150 microns.

DROPSIZE DISTRIBUTION RESULTS

The dropsize distributions produced by the secondary atomization process were also experimentally determined. Shown in Fig. 15 are five distributions obtained with the 0.094-inch diameter element at an injection velocity of 109 ft/sec. These data were obtained by varying the maximum gas velocity and show that the distribution becomes more nearly monodisperse as the gas velocity is increased, or equivalently, as the mass median dropsize becomes smaller.

This is especially evident when the percentage of mass in any particular dropsize group is examined. Shown in Fig. 16 is the mass fraction (in percent) that is contained in dropsize groups of 50-micron intervals for two of the distributions presented in Fig. 15. With a relatively large median dropsize, 318 microns, only about 10 percent of the mass is found in the 300- to 350-micron size group which contains the median dropsize. On the other hand, with the smaller median size of 128 microns, over 40 percent of the mass is contained in the size interval about the median dropsize, 100 to 150 microns.

It is possible that the absence of a large mass percentage of drops in the smaller size groups is due to either the impingement of the smaller drops with the test section walls, thereby being lost from the sample, or that they were being carried off the collection table by the high-velocity gas. However, as noted previously, the percentage of wax lost from the sample due to wax/wall impingement was intentionally increased to assess the impact on the distribution. It was found to have a negligible effect. Also, in a carefully controlled test to determine the amount of mass that was injected versus what was collected, it was found that about 10 percent of the mass could not be accounted for. Nevertheless, even if all of the droplets that were lost were in the 0- to 50-micron size group, it would not change the fact that most of the mass is concentrated in the size group about the mass median. The indications are, therefore, that the large drops in the spray (say >300 microns) are breaking up into what are still relatively large droplets of about 100 microns in diameter.

*Independent variation of $\overline{D}_o$ and the liquid flowrate was achieved by decreasing both d and V_L while maintaining constant $\overline{D}_o$ according to Eq. 1.

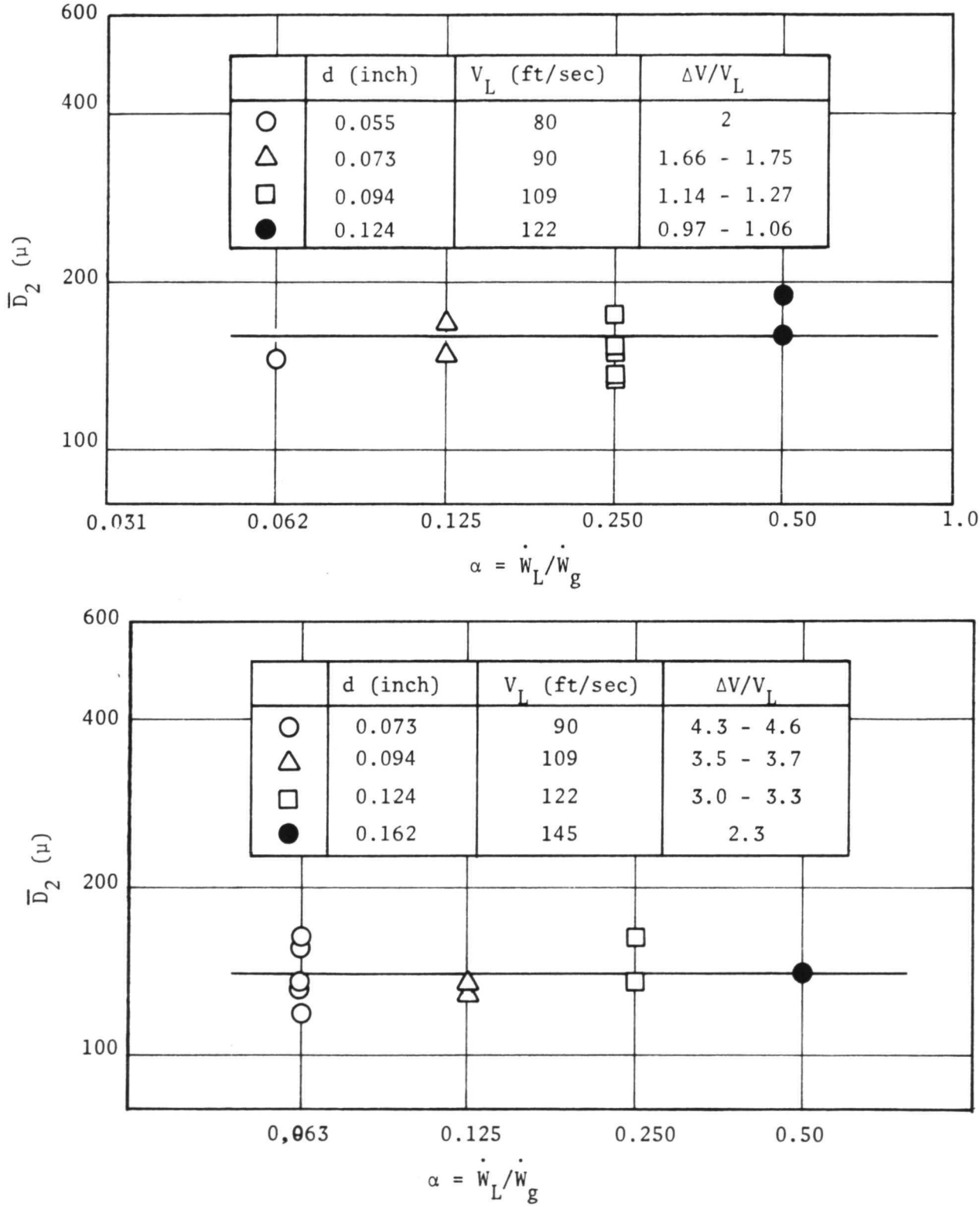

Figure 13. Influence of Liquid-to-Gas Mass Flux Ratio on the Mass Median Dropsize; $\overline{D}_o$ = 400 microns

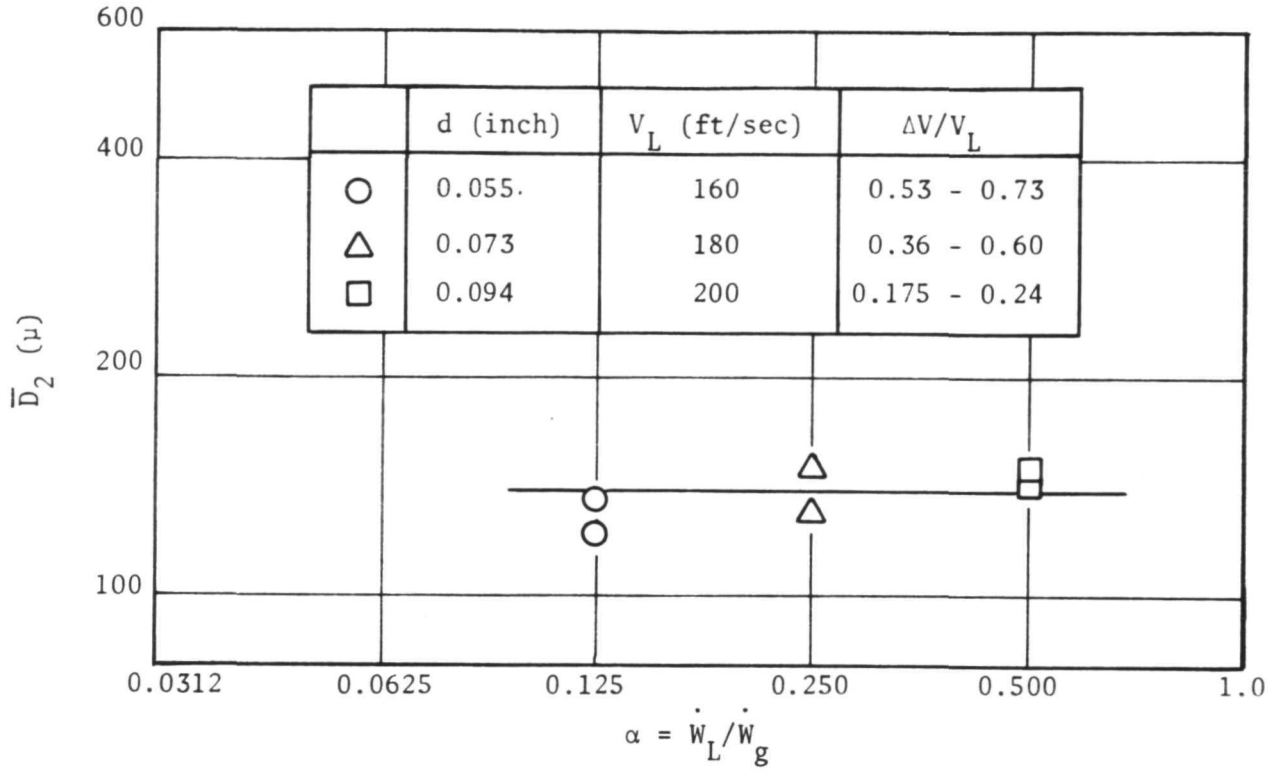

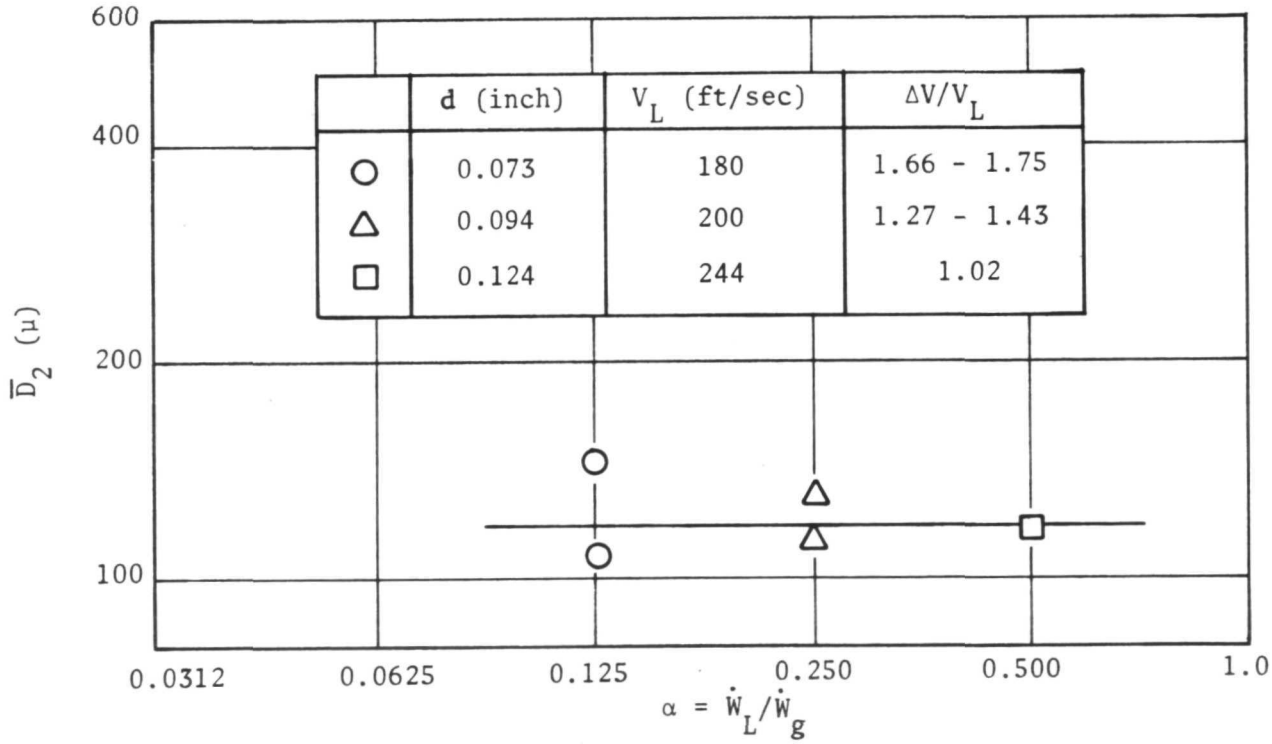

Figure 14. Influence of Liquid-to-Gas Mass Flux Ratio on the Mass Median Dropsize; $\bar{D}_o$ = 200 microns

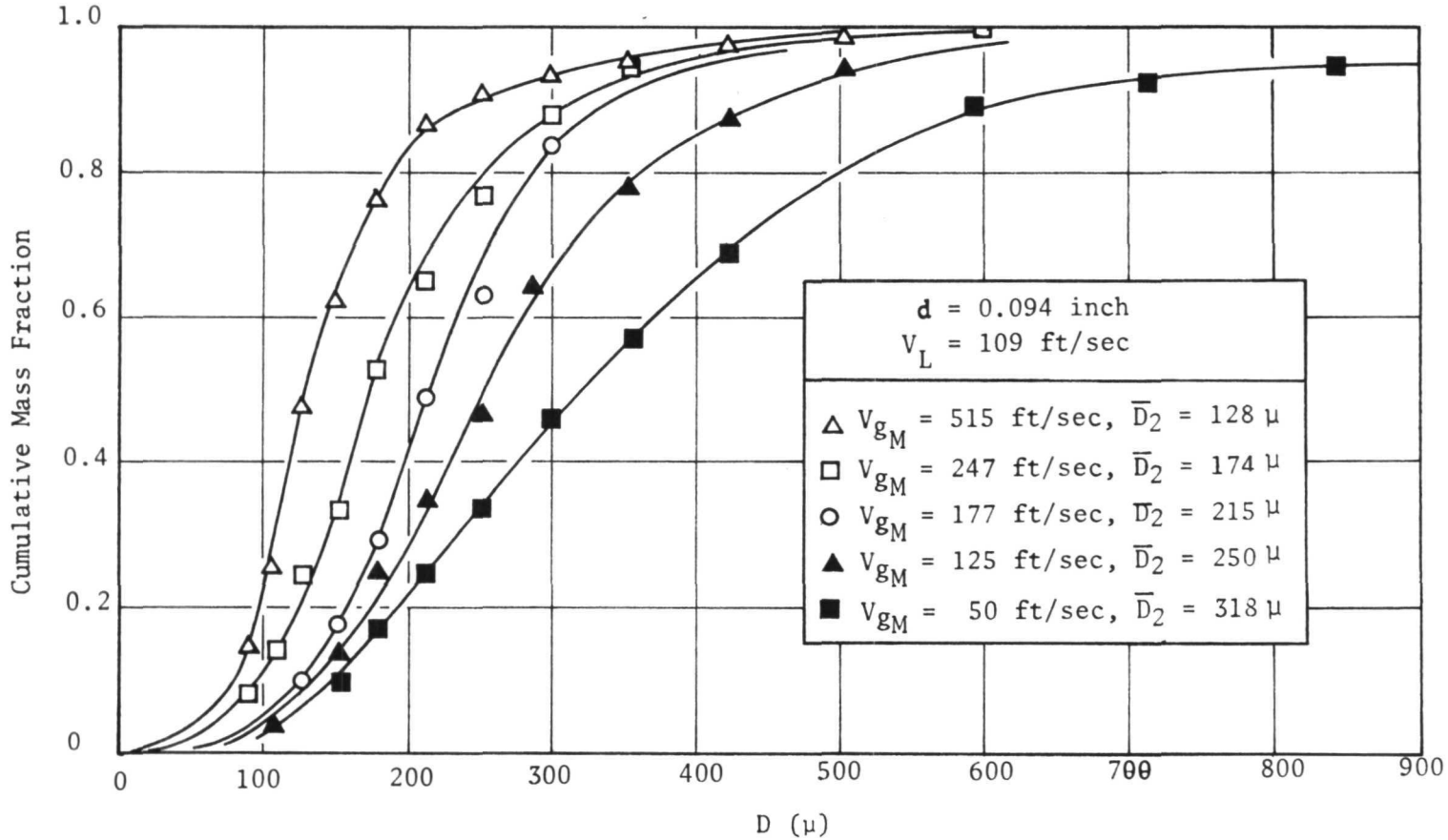

Figure 15. Dropsize Distributions Produced by Variations in Gas Velocity

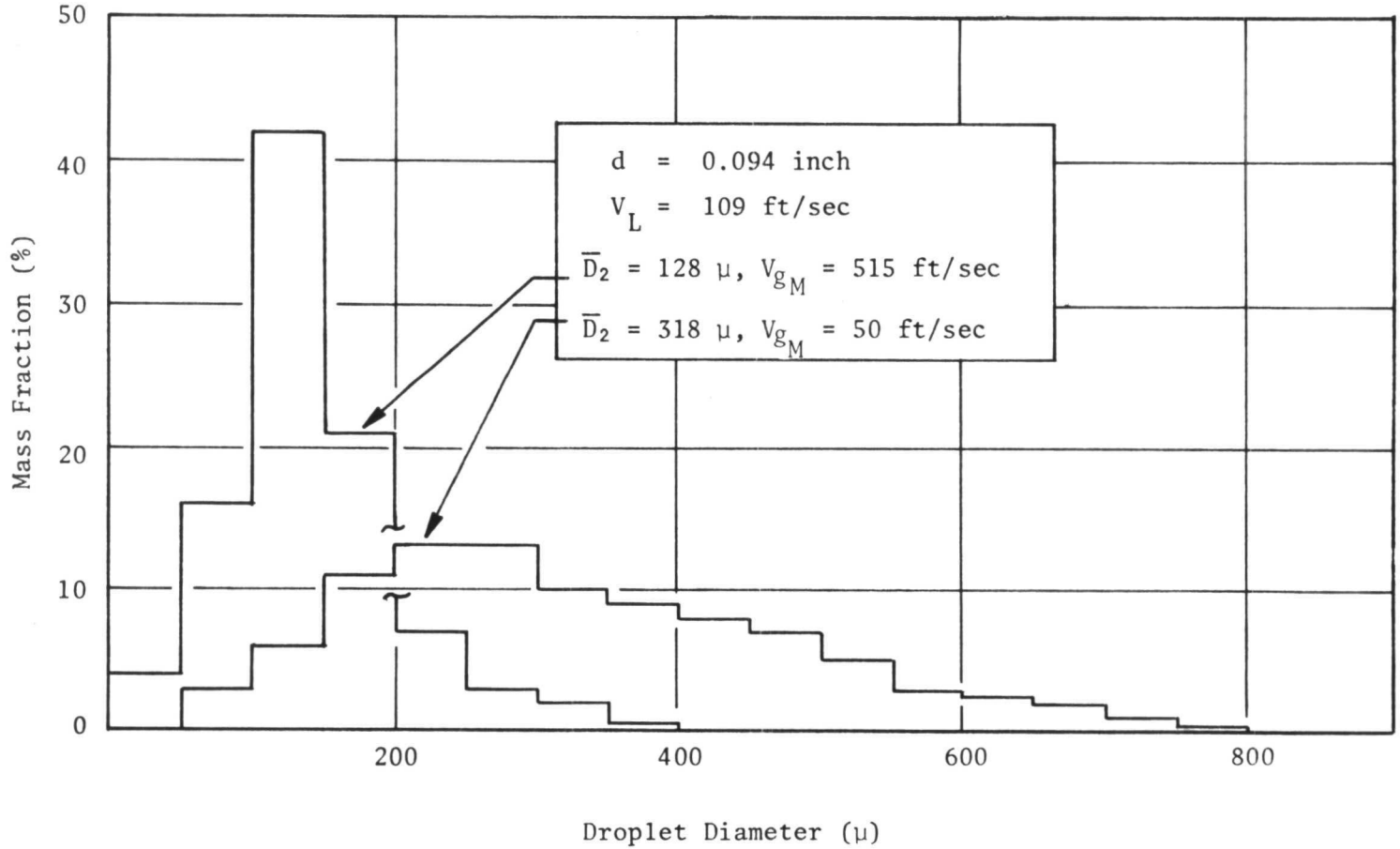

Figure 16. Mass Fraction of the Spray Versus the Droplet Diameter

Similar variations in the dropsize distributions were found when the gas velocity was varied with the other values of $\overline{D}_o$. Variations in L and/or α at otherwise constant conditions produced no change in the distribution.

A dropsize distribtuion function which was found to provide a reasonably good fit to all of the data was the Rosin-Rammler function (Ref. 12) given by:

$$\frac{d(\dot{w}/\dot{w}_T)}{d(D/\overline{D})} = \frac{2.46\ (D/\overline{D})^{1.46}}{(1.21)^{2.46}} \quad \exp\left(-\frac{(D/\overline{D})^{2.46}}{1.61}\right)$$

As shown in Fig. 17, this function agrees well with the normalized dropsize distribution of the larger median dropsize. It also agrees well with the upper portion of the distributions for the smaller mass median dropsizes. However, as the median dropsize decreases, the fit to the lower part of the curve becomes progressively worse. In terms of rocket engine application, this portion of the distribution is probably of lesser importance since the small drops would be rapidly vaporized in a combustion chamber and removed from the distribution. Therefore, accounting for the effect at secondary breakup on the mass median dropsize and using the Rosin-Rammler distribution, this is an acceptably valid way to estimate spray for combustion model input.

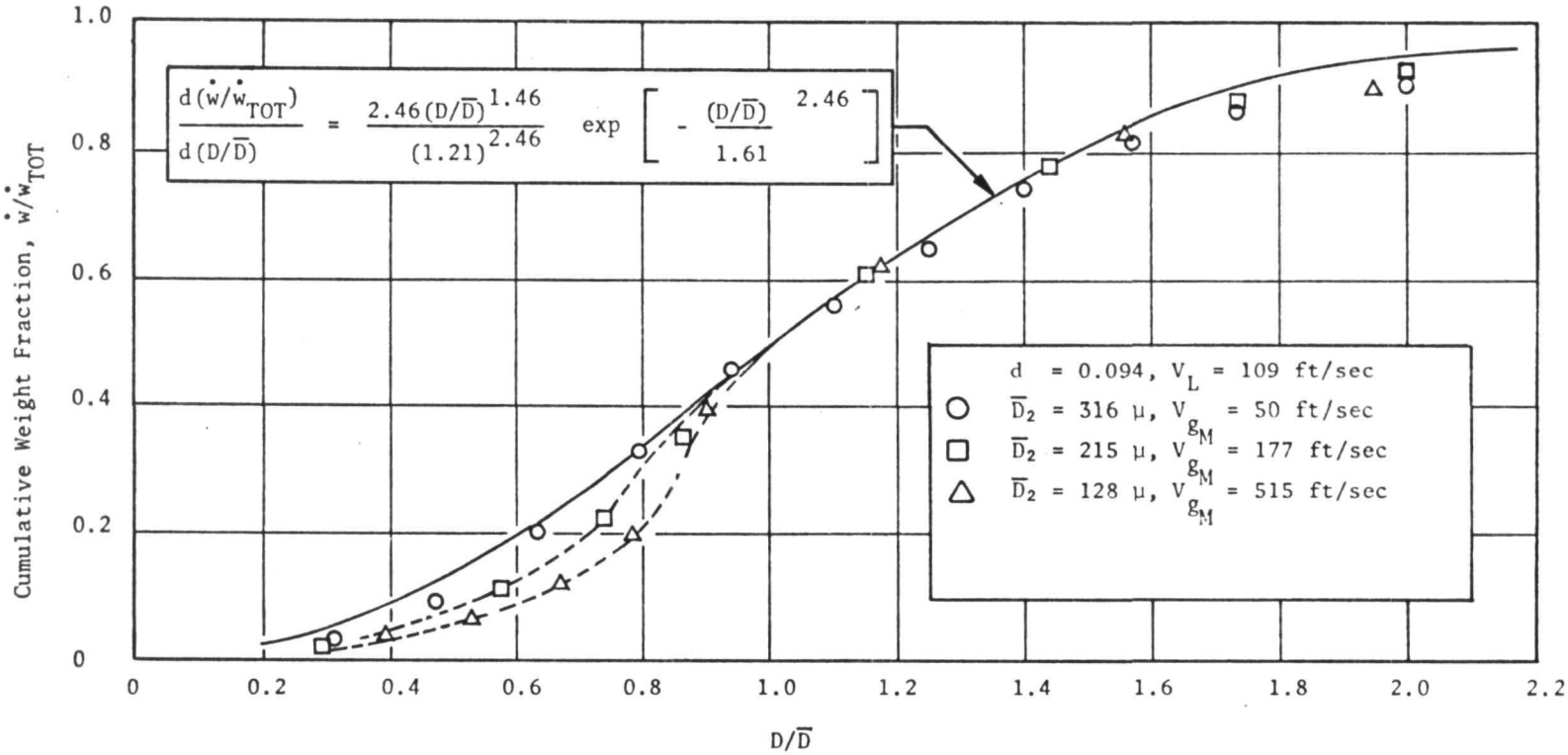

Figure 17. Comparison of Data to Rosin-Rammler Normalized Distribution Function

6.0 DISCUSSION

Single droplet breakup has been the subject of numerous investigations and criteria for the droplet breakup times and critical dropsizes have been developed as a result of these studies. However, in a liquid propellant rocket engine, dense sprays consisting of many droplets of various sizes are present. Application of a single droplet breakup criteria to these sprays to determine the dropsize distribution as the sprays proceed through the combustion chamber would require a sizeable effort. Even then, the results would be subject to question since the effects of particle shielding, spray distribution, and particle acceleration due to drag cannot be accurately taken into account.

Consequently, this study was primarily concerned with experimentally obtaining the median dropsizes and dropsize distributions that would be produced by the effects of a gas flow on sprays. These sprays were produced by injector elements that can be considered typical of rocket engine impinging stream injectors. Accelerating gas flows which were also utilized. Therefore, these data should be directly applicable to rocket engine performance calculations.

EMPIRICAL CORRELATION OF RESULTS

To present the results in a form that can be readily incorporated into a combustion model computer program for performance calculations, empirical equations in terms of the basic experimental parameters were developed. The parameters that were found to have the largest effect on the median dropsize were the injector parameters of diameter, d, and velocity, V_L, and the maximum gas velocity experienced by the spray, V_{g_M}. Consequently, these were the parameters considered in the correlations. No single function could be determined that would accurately fit all of the data over the entire range of the parameters. Therefore, two functions, one for the low gas velocity regime and a second for the high gas velocity regime, were developed.

For small gas velocities, the following function was found to provide the best fit to the data*:

$$\overline{D}_2 = \overline{D}_c \left[1 - 1.77\text{x}10^{-3}\, \overline{D}_c \frac{\Delta V}{V_L} \exp\left(-0.24 \frac{\Delta V}{V_L} \left| \frac{\Delta V}{V_L} \right| \right) \right] \tag{2}$$

where

$$\frac{\Delta V}{V_L} = \frac{V_{g_M} - V_L}{V_L} \tag{3}$$

and

$$\overline{D}_c = 2.2\text{x}10^4\, d^{0.375}/V_L^{0.75} \tag{4}$$

*$\overline{D}_2$ and $\overline{D}_c$ in microns, V_{g_M} and V_L in ft/sec, and d in inches

In Eq. 2 , $\Delta V/V_L$ should be limited to the range $-1 < \frac{\Delta V}{V_L} \leq 1.25$. At higher gas velocities, $\Delta V/V > 1.25$, the function:

$$\bar{D}_2 = \bar{D}_c \left[1 - 7x10^{-5} \bar{D}_c \right] -12 \ln\left(\frac{\Delta V}{V_L}\right) \qquad (5)$$

was found to provide a good fit to the data.

In the above, $\bar{D}_2$ is, of course, the mass median dropsize of the spray after the spray has been exposed to the gas flow. As can be seen from inspection of Eq. 2 , $\bar{D}_c$ is the mean dropsize obtained at a condition of zero ΔV.

The solid lines drawn through the data in Fig. 9 through 12 were determined from the above correlations. As can be seen there, Eq. 2 and 5 provide an excellent fit to the data.

It was previously noted that the median dropsize that would be obtained from the injectors in still air, $\bar{D}_o$, can be expressed by Eq. 1 , i.e.:

$$\bar{D}_o = 15.9 \times 10^4 \, d^{0.57}/V_L$$

If this function is substituted into Eq. 4 , the dropsize, $\bar{D}_c$, becomes:

$$\bar{D}_c = 8 \, \bar{D}_o^{0.66}/V_L^{0.09} \qquad (6)$$

Thus, if the small effect of V_L in Eq. 6 is neglected, the secondary dropsize, $\bar{D}_2$, is seen to be a function of the characteristic dropsize of the injector, $\bar{D}_o$, and the nondimensional velocity, $\Delta V/V_L$.

The parameter, $\Delta V/V_L$, was particularly useful in collapsing the data obtained at low gas velocities. This is evident if one considers that, as the gas velocity approaches zero, the dropsize $\bar{D}_2$ should approach $\bar{D}_o$. Hence, Eq. 2 should become independent of V_L. The parameter $\Delta V/V_L$ achieves this since $\Delta V/V_L \longrightarrow -1$ when $V_g \longrightarrow 0$.

The "secondary" dropsize, $\bar{D}_2$, as determined from the empirical correlations (Eq. 2 and 5), is shown in Fig. 18 as a function of the characteristic dropsize, $\bar{D}_o$, for various values of the parameter $\Delta V/V_L$ greater than -1. (For $\Delta V/V_L = -1$, $\bar{D}_2 \equiv \bar{D}_o$ independent from the value of V_L.) Figure 18 thus summarizes the results of this study. As shown there, the dropsize, $\bar{D}_2$, decreases as the gas velocity is increased with fixed injector parameters, i.e., constant $\bar{D}_o$ and V_L. It also shows that a limiting value of $\bar{D}_2$ is obtained as both $\bar{D}_o$ and $\Delta V/V_L$ are increased. The effect of V_L, independent of its contribution to $\bar{D}_o$ and $\Delta V/V_L$, is seen (dashed lines in Fig. 18) to be small for low values of $\Delta V/V_L$, and totally negligible for large values of $\Delta V/V_L$.

As noted previously, the dropsize distributions were found to correlate well with the normalized distribution function given by:

$$\frac{d(\dot{w}/\dot{w}_T)}{d(D/\bar{D})} = \frac{2.46 \ (D/\bar{D})^{1.46}}{(1.21)^{2.46}} \exp\left(-\frac{(D/\bar{D})^{2.46}}{1.61}\right)$$

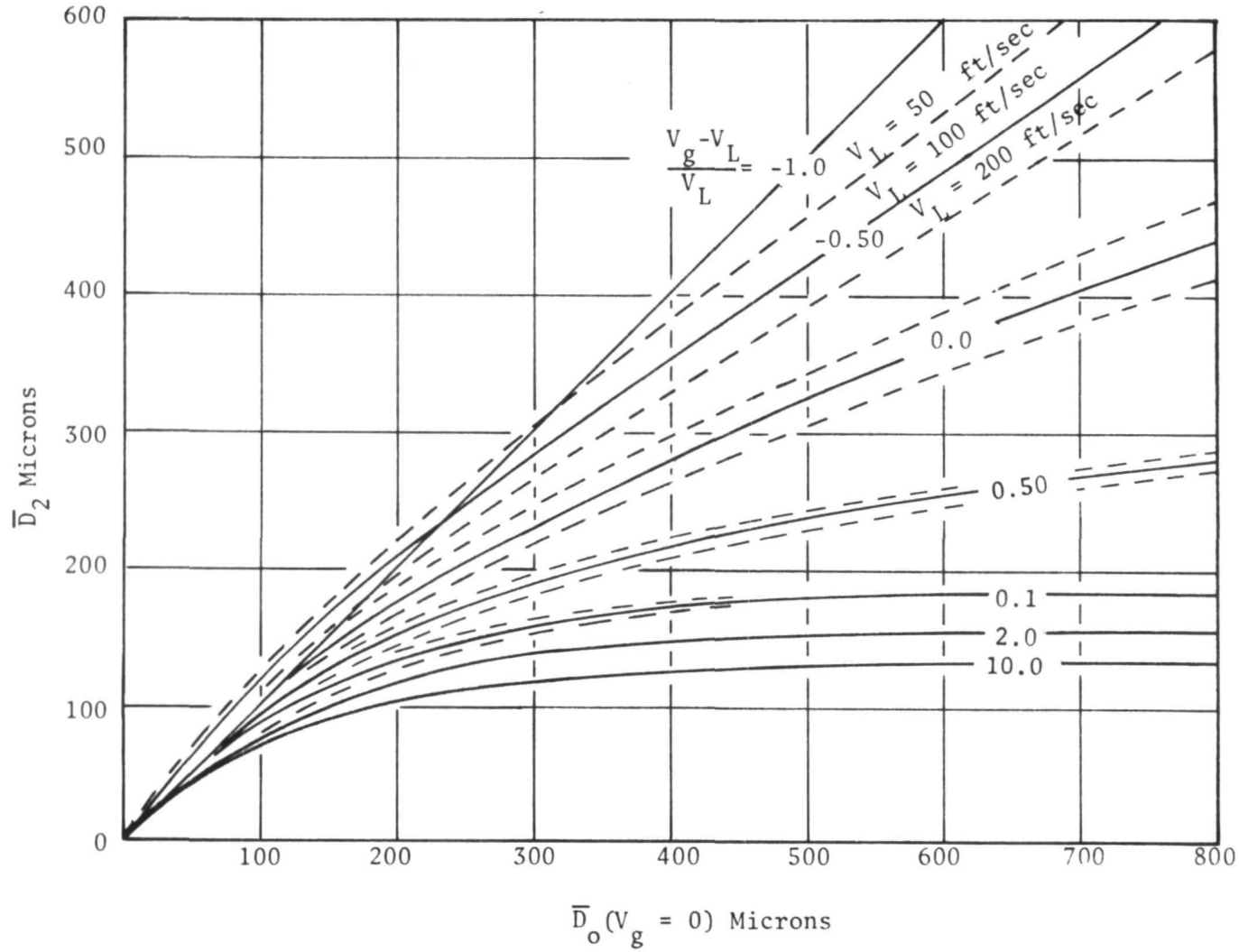

Figure 18. Plot of the Empirical Correlations

The basic form of this function was suggested by Rosin and Rammler (Ref. 12).

The above distribution, together with the empirical correlations (Eq. 2 and 5), are sufficient to completely characterize the dropsize distribution over the range of experimental parameters examined.

Equations 2 and 5 should not be employed outside of the ranges in which data were obtained. Specifically, $\overline{D}_o$ should be limited to values of from 200 to about 600 microns. In terms of $\overline{D}_c$, which incorporates the range of orifice diameters and injection velocities examined, the limits should be $140 \leq \overline{D}_c \leq 360$. Most rocket engine injectors will have values of these parameters within the prescribed ranges.

SALIENT FEATURES OF THE RESULTS

The results have demonstrated that, under conditions simulating those of typical rocket engine combustion chambers, a significant amount of atomization will occur because of gas velocity effects on the spray. In addition, however, the results have also shown that: (1) the spray density, defined as the liquid-to-gas mass flux ratio, did not appear to effect the results over the range of flowrates examined; (2) the results could be correlated in terms of the maximum gas velocity achieved by the flow, which suggests that the breakup times are extremely short; (3) the distance over which the gas is accelerated had a small effect on the results; and (4) the dropsize obtained with fixed injector parameters approached a limiting value at large gas velocities.

The liquid-to-gas mass flux ratio, α, was selected as an experimental parameter because it is a qualitative measure of the spacing of the droplets. It is qualitative in the sense that variations in α imply the direction of change in the droplet spacing even though the absolute spacings of the droplets in the spray are not known. (For example, an increase in α, representing more liquid for a given gas flowrate, would imply more closely spaced drops.) An observed effect of α on the dropsize would then indicate that the forces exerted on the droplets were being changed because of variations in the droplet spacing. However, since no effect was observed, it must be concluded that the droplet surface shear forces are a weak function of droplet spacing in the regime studied.

If it is assumed that: (1) all of the liquid droplets are the same diameter, (2) they are uniformly distributed throughout the gas flowfield, and (3) their velocities are equal and are unaffected by the gas, the average spacing of the droplets can be expressed as:

$$\frac{S}{\overline{D}} = \sqrt[3]{\frac{\pi A_c \rho_L V_L}{6 \dot{w}_L}} = \sqrt[3]{\frac{\pi A_c \rho_L V_L}{6 \alpha \dot{w}_g}} \qquad (7)$$

where A_c is the cross-section area of the flowfield and ρ_L is the liquid density (47.7 lb/ft^3). For the flowrates and velocities examined in this study, S/D ranged from about 6 to 13 at the throat of the test section (A_c = 20 in.^{2})*.

*This represents a lower limit on the spacing since droplet acceleration would tend to increase S/D.

Shown in Fig. 19 is the drag force (relative to infinitely space particles) as a function of particle spacing that was determined by Rowe (Ref. 13). Rowe's results tend to support the conclusion made here in that, as shown in Fig. 19, the drag force was found to be a slowly varying function of particle spacing when X/D = S/D-1 was greater than about 5.

The observed independence of the results on the particle spacing does not, however, imply that the results could have been deduced from single droplet breakup criteria. When the results were compared to single droplet breakup criteria found in the literature, it was found that the measured dropsizes were larger than would be predicted from these criteria. For example, using the criteria developed by Gordon* (Ref. 7), the largest dropsize that would be present in the spray at a relative gas/liquid velocity of 180 ft/sec would be found to be about 100 microns. This dropsize is smaller than even the mean dropsize actually measured for a similar relative velocity. Thus, the fact that the particles have a finite spacing indicates that there is less droplet breakup occurring than would be obtained if the drops were infinitely spaced apart. This suggests a shielding effect in which the droplets "protect" each other from the action of the gas by one droplet following in the wake of another.

This shielding effect would retard droplet breakup by reducing the relative gas-to-droplet velocity for some fraction of the drops. In essence, there would then be a relative velocity distribution for drops of a given size. That is, some drops of 200-micron diameter would be experiencing a force sufficient for breakup while the remainder would not. The influence of droplet shielding, however, appears to be relatively constant over the spray densities (i.e., particle spacings) examined. This is consistent with the suggestion of a relatively constant drag force (from Fig. 19) over the range of S/D examined, although the force may be larger than that of infinitely spaced particles.

As noted above, the results also indicate that the breakup time of the droplets in the spray is much shorter than the residence time in the test section. Two factors suggest this. First, only a negligibly small effect on dropsize of the length of the acceleration zone was observed. This result is consistent with single droplet breakup criteria in terms of at least the order of magnitude of the breakup time if, perhaps, not the absolute value. For example, with a gas/liquid relative velocity of 300 ft/sec, the breakup criteria of Gordon (Ref. 7) would yield a breakup time of about 10 microseconds for any drop exceeding 100 microns in diameter. In comparison, a droplet traveling at 100 ft/sec has a 1700-microseconds residence time in the 2-inch acceleration zone. Thus, even if the breakup time of droplets in a spray were an order of magnitude longer than that of a single droplet, the time required for breakup would still be small compared to the "available" breakup time.

Second, the constant gas velocity and accelerating gas flow tests yielded the same dropsize when compared on the basis of equal maximum gas velocities. In the accelerating flow case, the maximum gas velocity exists only instantaneously at the throat of the test section. If, however, the test section length over

*Gordon's work was selected as a basis of comparison since the criteria allow the effects of physical properties to be included in the estimation of critical dropsize, breakup time, etc.

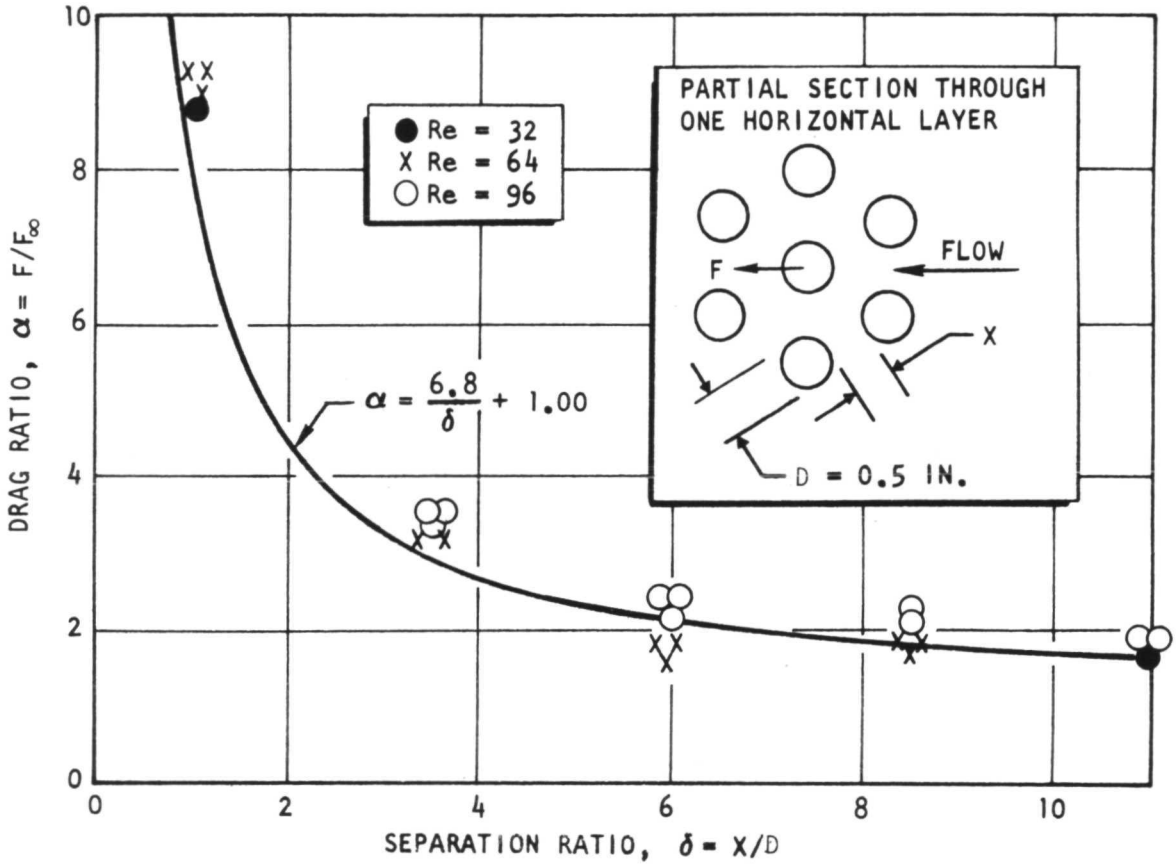

Figure 19. Variation of Drag Ratio With Separation (Ref. 13)

which V_g lies between 0.9 V_{g_M} and V_{g_M} is determined, it is found that it is approximately 5 percent of the length of the acceleration zone. Neglecting droplet acceleration and considering again the 2-inch section, the time for a droplet traveling 100 ft/sec to traverse the maximum gas velocity "region" (0.1 inch) would be about 85 microseconds. This time can thus be considered as an approximate (and probably upper limit) breakup time of droplets in sprays of similar droplet number density and droplet size to those examined in this study.

Since the distances, velocities, rates of acceleration, and spray densities in the dropsize experiments are similar to those encountered in typical rocket engine combustion chambers, the residence times are also comparable. Thus, neglecting breakup time under combustion chamber conditions would be a reasonable assumption.

The empirical correlations presented above do not explicity contain the fact that the gas was accelerating. However, the gas acceleration effects are implicit in the results since the measured dropsizes are commensurate with the actual gas/droplet relative velocity, even though the correlations are expressed in terms of the maximum gas velocity and liquid injection velocity.

Nevertheless, to determine the potential effects of particle drag on the results, a series of calculations was performed to determine, approximately, the amount of acceleration the droplets would experience. For these calculations, the "standard" solid sphere drag law given by:

$$C_D = \frac{24}{Re}\left[1 + \frac{(Re)^{2/3}}{6}\right] \qquad (8)$$

where Re is the Reynold number, was assumed. No correction was made to account for the effects of particle spacing on the drag although (as shown in Fig. 19) a somewhat larger drag force would be expected than would be given by Eq. 8 .

The drop velocity, V_D, as a function of the distance downstream of the start of the gas acceleration zone, X, was determined by numerically integrating the following equation:

$$\frac{d\,V_D}{dX} = \frac{3}{4}\,\frac{C_D\,\rho_L\,(V_g - V_D)\left|V_g - V_D\right|}{D\,V_D} \qquad (9)$$

between the limits $0 \leq X \leq L$ where L is the distance over which the gas undergoes acceleration. The gas velocity was assumed to be unaffected by the liquid drops and was determined from one-dimensional gas dynamic theory for a perfect gas.

Equation 9 was solved for the nominal values of experimental gas flowrates, i.e., 2, 4, and 8 lb/sec, through the 5:1 contraction ratio test section. These flowrates correspond to initial (X = 0) to maximum (X = L) gas velocities of 50 to 250, 100 to 500 and 150 to 950 ft/sec, respectively. Each of these maximum gas velocities was achieved over distances, L, of 2, 4, 8, and 16 inches. Therefore, the acceleration of the gas at a constant gas flowrate

was a function of L. For values of X larger than L, the gas is decelerated within the diffuser. The gas velocity profiles in the diffuser for the three flowrates considered in the calculations were previously shown in Fig. 4. The liquid velocity at X = 0 was taken to be 100 ft/sec for all cases and is assumed to be the liquid injection velocity.

A typical result is shown in Fig. 20, where the velocities of the gas and of drops ranging in size from 100 to 1000 microns are shown as functions of X. This calculation corresponds to an 8 lb/sec gas flowrate and an acceleration length, L, of 8 inches. Figure 20 shows that a considerable acceleration of the drops can occur, thereby producing a droplet velocity substantially different from the injection velocity. For example, the maximum gas/liuqid ΔV based on the droplet velocity, V_D, is about one-half the ΔV based on the injection velocity. Figure 20 also shows the obvious result of greater acceleration of the smaller droplets.

Figure 21 represents a compilation of all the calculations. It shows the calculated gas-to-droplet velocity difference as a function of the gas-to-injection velocity difference over the range of acceleration distances considered. The results are shown for 100- and 300-micron drops. These results should, of course, be viewed as qualitative since the absolute numbers are critically dependent on the value of the drag coefficient chosen. (For example, larger drag coefficients would reduce the realizable value of $V_{g_M} - V_D$.) Nevertheless, the figure illustrates several potential effects of the accelerating gas flow on the results.

First, at low maximum gas velocities ($V_{g_M} - V_L \lesssim 100$ ft/sec), the droplets experience little acceleration. This result, in conjunction with the assumption of short breakup time, explains why the constant velocity and accelerating gas flow tests yielded the same results in the low gas velocity regime where common data were obtained.

At high gas velocities, it can be seen that considerable acceleration is experienced by the droplets, i.e., $V_D \gg V_L$. For example, $V_{g_M} - V_D$ is about 540 ft/sec for L = 2 inches, and 400 ft/sec for L = 16 inches, as compared to a value of $V_{g_M} - V_L$ of 800 ft/sec. It can also be seen that large increases in $V_{g_M} - V_L$ are required to increase $V_{g_M} - V_D$. Thus, part of the reason for the apparent limiting dropsize (as shown in Fig. 9) is due to a limit on the realizable value of the gas-to-droplet relative velocity.

However, a second reason for the apparent limit in dropsize is that as the dropsize decreases as a result of gas action, increasingly greater values of ΔV are required to cause further breakup (Ref. 7). At the same time, as shown in Fig. 21, the realizable value of ΔV (i.e., $V_g - V_D$) decreases as the dropsize gets smaller, e.g., the difference between D = 300 microns and D = 100 microns. Thus, in an accelerating flowfield, this tradeoff apparently results in a lower limit of the mean dropsize.

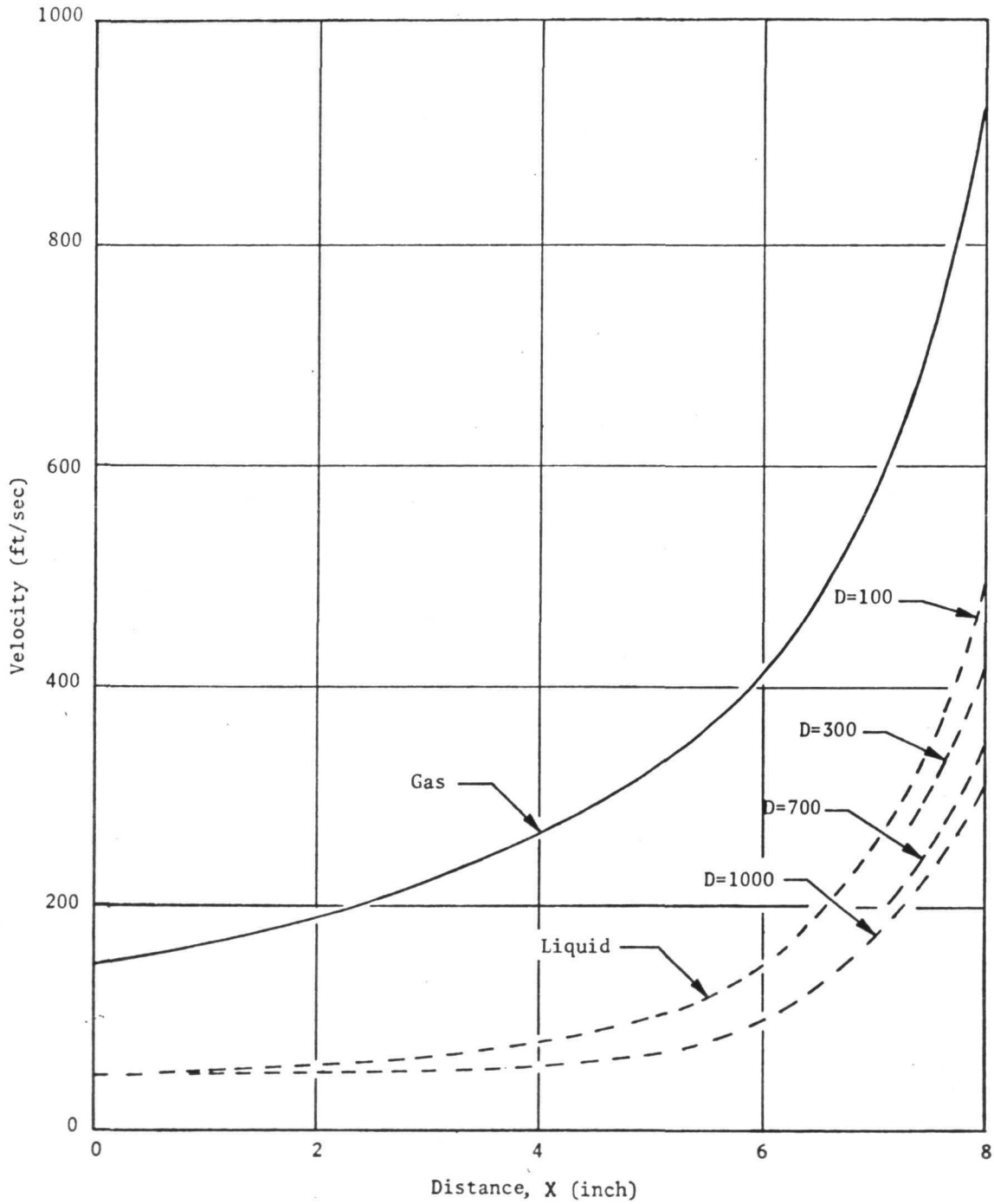

Figure 20. Typical Result of Droplet Drag Calculation

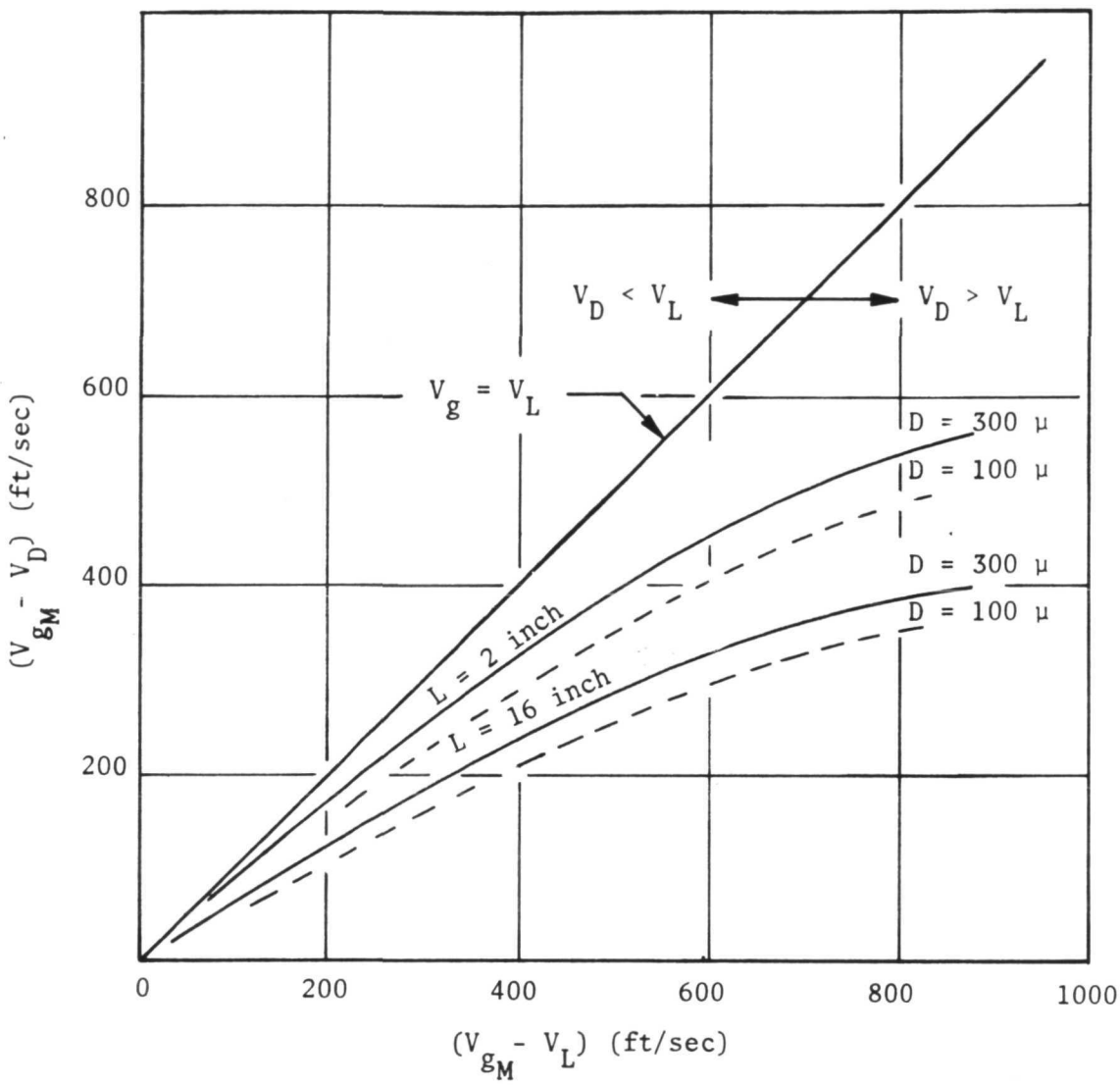

Figure 21. Comparison of the Calculated Drop Velocity to the Liquid Injection Velocity

APPLICATION OF RESULTS TO COMBUSTION MODELS

The incorporation of the empirical correlations presented above into an existing combustion model was beyond the scope of the current program. However, it is recommended that the initial approach to incorporating the effects of the gas velocity on droplet breakup should be simply an overall correction to the median dropsize. This would require the least amount of time in terms of programming and operation.

With this approach, the combustion model would be run twice. First, using dropsize correlations that yield the median dropsize in a static environment (e.g., Eq. 1) the gas velocity at the entrance to the nozzle is computed. Then, using this gas velocity, a correction to the median dropsize is obtained from the above empirical functions. The combustion model computer code is then run again with the corrected dropsize. The normalized dropsize distribution would be assumed invariant in accordance with the results obtained here.

A more sophisticated approach would be to correct the dropsize at many intervals throughout the computation. However, this approach is more expensive to program and run and, unless a comparison of calculated (using the simpler approach) and measured performance indicates that it may be necessary to do this, it is not recommended.

Page Intentionally Left Blank

7.0 CONCLUDING REMARKS AND RECOMMENDATIONS

The objective of this study was to examine the secondary atomization of clouds of droplets under an accelerating gas flow and develop, from the experimental data, an empirical correlation for the median dropsize in terms of the experimental variables. This objective was achieved.

The experimental parameters and their magnitudes were chosen so as to simulate, as closely as possible, the dropsizes, spray densities, velocities, chamber lengths, and rates of acceleration realized in typical rocket engine combustion chambers. The results should, therefore, be directly applicable to combustion model calculations of the performance of such engines.

On the basis of the experimental results, it is concluded that a substantial amount of spray droplet breakup will occur as a result of gas velocity effects. Neglecting this additional atomization could result in an underestimation of the combustion efficiency.

It is further concluded that the parameters that will most affect the resulting median dropsize are the injector parameters of orifice diameter and injection velocity and the maximum gas velocity. Little or no effect of the remaining two experimental parameters, i.e., the distance over which the gas acceleration occurred and the liquid-to-gas mass flux ratio, was observed. This latter conclusion applies only to the range of the parameters studied here.

In addition, the results indicate that, while an accelerating gas acting on a cloud of liquid droplets will enhance atomization, the amount of spray droplet breakup is less than what would be expected from single droplet breakup criteria. Furthermore, the results suggest that the breakup time for droplets in a spray is small compared to the residence times of droplets in typical combustion chambers. Exposing the drops to an accelerating gas, as opposed to a constant velocity gas flow, appears to result in a limiting dropsize since, because of droplet acceleration, the high relative gas/liquid velocities required for additional breakup cannot be attained.

Lastly, it can be concluded that the molten wax technique employed in this study is a viable experimental technique for the evaluation of droplet breakup in gaseous flowfields.

The experimental program conducted in this study was exploratory in the sense that only one injector type was considered and that wide ranges of only a few experimental parameters were examined. The results have, however, provided information that is immediately useful in combustion model computer codes,* and, also, have delineated the important experimental parameters and the ranges of these parameters in which future studies should be concentrated.

Specifically, the following recommendations for future effort are:

1. Incorporation of the empirical correlations presented here into existing combustion model computer codes. This would allow a "first step"

* See also Ref. 9

improvement of combustion model performance calculations. The adequacy of the correlations could be judged by a comparison of existing experimental performance data to that obtained when droplet breakup is accounted for in the calculated performance.

2. Other injector element types should be examined. Since the droplet breakup of impinging-stream types, e.g., triplets, pentads, etc., will probably be similar to the like doublet studied here, future effort should be directed mainly toward injector concepts such as the concentric tube or showerhead.

3. Future experimental studies should also be concentrated in the low gas velocity regime, i.e., less than 1 to 2 times the liquid velocity. The results obtained here indicate that this is where most of the droplet breakup occurs.

4. Additional experiments at both larger and smaller (approaching infinitely spaced particles) values of the liquid-to-gas mass flux ratio would also be of interest. This would provide more information on the possible influence of droplet shielding on breakup.

5. The effects of both the liquid physical properties and the gas physical properties should be examined. As a start, this could be readily achieved through the use of waxes with different viscosities and with helium/nitrogen mixtures to vary the gas properties.

APPENDIX A

PARTICLE SAMPLE ANALYSIS

The following procedure was used for the analysis of the wax samples:

1. A 100-gram sample of wax particles was placed in a Buchner funnel and subjected to suction for removal of water.
2. After the particles had been partly dried by suction, they were placed on a large tray in a vacuum chamber for a period of at least 48 hours to ensure that the particles were completely dry.
3. After drying, a random 10-gram sample was selected to be sieved. A series of 23 standard testing sieves ranging in size from 53 to 2380 microns was used. For any paticular sample, only 12 of the sieves were used; the particular sieve sizes used depended on the anticipated size range of the particle sample. The sieves were shaken on a "RO-TAP" automatic sieve shaker for 30 minutes, during which time the shaking was stopped every 6 minutes and each sieve struck sharply several times to help release any particles which had become wedged in the sieve screens.
4. After the sieving operation was completed, the mass of particles retained on each sieve was weighed on an electric balance. It was found that with considerable care in transferring the wax from the sieves into the weighing pan, a total recovery of 97 to 99 percent of the mass originally introduced into the sieves was possible. The photographs shown in Fig. A-1 are typical of the uniformity of sizes of the solid wax particles obtained by the sieving operation.
5. These data were then converted into the total fraction of mass having a particle size smaller than each of the sieve sizes. An example of the raw data and converted data is shown in Table A-1. The data shown in Table A-1 are also shown plotted in Fig. A-2.

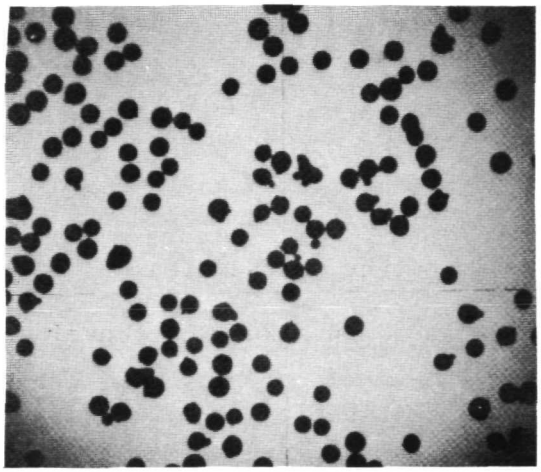

500 Microns

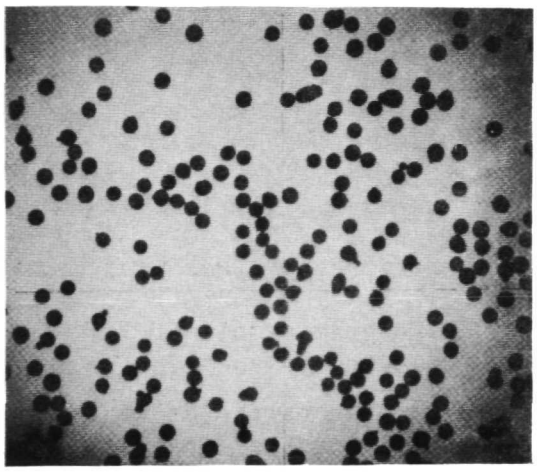

420 Microns

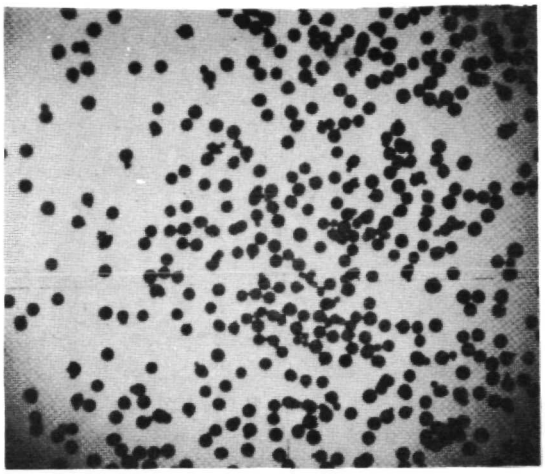

354 Microns

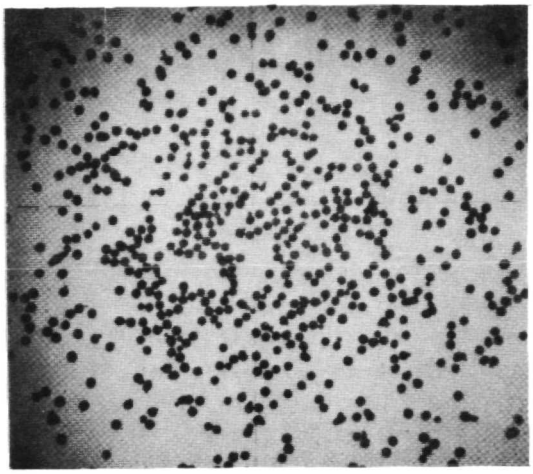

250 Microns

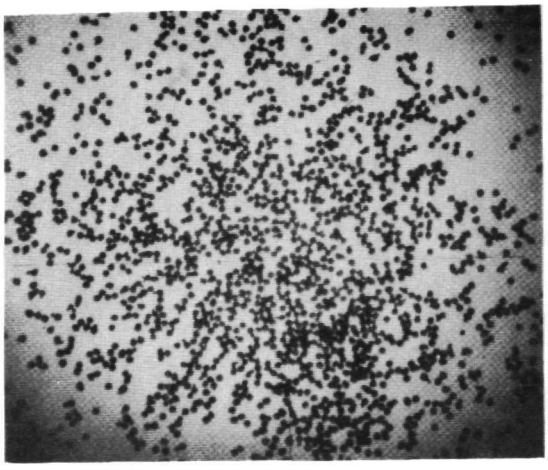

177 Microns

125 Microns

Figure A-1. Photographs of Solidified Wax Droplets Using a 0.063-Inch-Diameter Like-Doublet Element

TABLE A-1. TYPICAL RESULTS FROM SIEVING ANALYSIS*

Sieve Size, microns	Mass in Sieve, grams	Fraction of Total Mass	Cumulative Fraction of Total Mass Having Particle Size Smaller Than Sieve Size
Catch Pan	0.156	0.0153	--
88	0.139	0.0141	0.0153
105	0.169	0.0170	0.0293
125	0.208	0.0211	0.0464
149	0.667	0.0674	0.0674
177	0.591	0.0598	0.1348
210	1.042	0.1053	0.1946
250	1.201	0.1214	0.2999
297	1.490	0.1507	0.4212
354	1.609	0.1627	0.5719
420	1.138	0.1150	0.7346
500	1.155	0.1168	0.8496
590	0.332	0.0336	0.9664

*0.063-inch-diameter like-doublet injector with free jet length of 5 diameters and ΔP = 100 psi

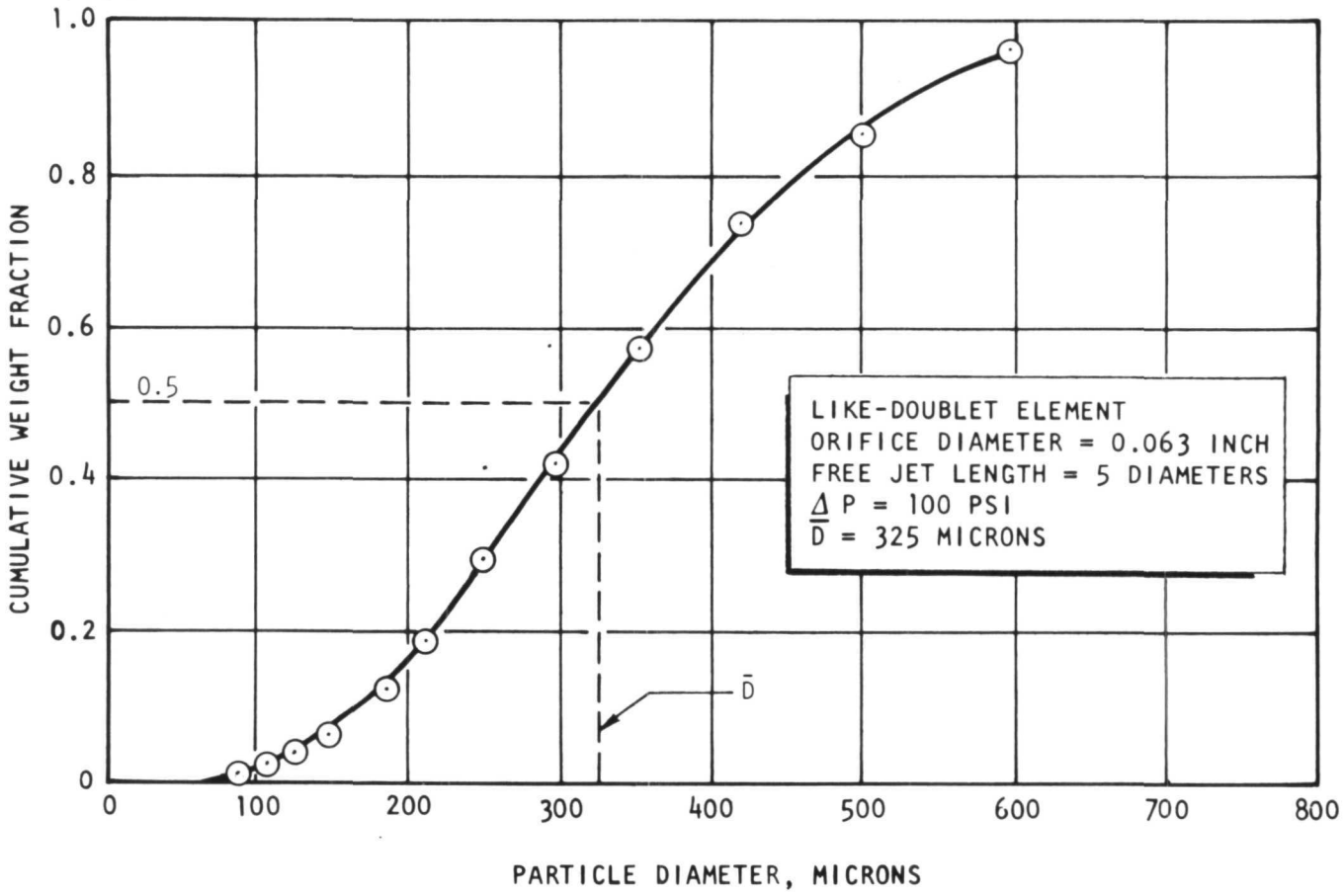

Figure A-2. Typical Particle Size Distribution Data Obtained Using the Frozen Wax Technique

APPENDIX B

REFERENCES

1. Priem, R. J., and M. F. Heidmann, Propellant Vaporization as a Design Criterion for Rocket Engine Combustion Chambers, NASA TR R-67, National Aeronautics and Space Administration, Washington, D.C., 1960

2. Lambiris, S., L. Combs, and R. Levine, "Stable Combustion Process in Liquid Rocket Engines," Combustion and Propulsion, Fifth AGARD Colloquium, High Temperature Phenomena, pp 569-634, MacMillian, New York, N.Y., 1963.

3. Dickerson, R. A., K. Tate and W. H. Nurick, Correlation of Spray Injector Parameters With Rocket Engine Performance, AFRPL-TR-68-11, Rocketdyne, a Division of Rockwell International, Canoga Park, California, January 1968.

4. Reibling, R. W., R. M. Knight, and C. K. Nagai, Chamber Technology for Space Storable Propellants, Task II, Interim Report, Vol. 2, R-6028-2, Rocketdyne, a Division of Rockwell International, Canoga Park, California, October 1965.

5. Dickerson, R. A., and T. A. Coultas, Breakup of Droplets in an Acclerating Gas Flow, AIAA Paper 66-611, AIAA Second Propulsion Joint Specialist Conference, Colorado Springs, Colorado, June 1966.

6. Lane, W. R., "Shatter of Drops in Streams of Air," J. of Ind. and Eng. Chemistry, Vol. 43, No. 6, 1312-1317, June 1951.

7. Gordon, G. D., "Mechanism and Speed of Breakup of Drops," J. of Applied Physics, Vol. 30, No. 11, 1759-1761, November 1959.

8. Ingebo, R. D., Dropsize Distributions for Impinging-Jet Breakup in Air-Streams Simulating the Velocity Conditions in Rocket Combustors, NACA TN 4222, National Advistory Committee For Aeronautics, Washington, D.C., March 1958.

9. Zajac, L. J., Droplet Breakup in Accelerating Gas Flows, Part I: Primary Atomization, NASA CR-13478, Rocketdyne, a Division of Rockwell International, Canoga Park, California, October 1973.

10. Zajac, L. J., Correlation of Spray Dropsize Distribution and Injector Variables, Rocketdyne, a Division of Rockwell International, Canoga Park, California, February 1971.

11. Yeo, D., J. Agric. Engng. Res., 4, No. 2, 1961.

12. Rosin, P., and E. Z. Rammler, Ver. Duet. Ing., 71, 1, 1927, J. Inst. Fuel, 1, 29, 1933.

13. Rowe, P. N., "Drag Forces in a Hydraulic Model of a Fluidized Bed - Part II," Trans. Instn. Chem. Engrs., Vol. 39, 175-180, 1961.

Page Intentionally Left Blank

APPENDIX C

DISTRIBUTION LIST (CONTRACT NAS3-14371)

	Copies
National Aeronautics and Space Administration Lewis Research Center 21000 Brookpark Road Cleveland, Ohio 44135	1
Attn: Dr. R. J. Priem MS 500-209	2
N. T. Musial MS 500-311	1
Library MS 60-3	1
Report Control Office MS 5-5	1
L. Gordon, MS 500-209	1
E. O. Bourke MS 500-209	1
Rockets and Spacecraft Procurement Section MS 500-313	1
E. W. Conrad MS 500-204	1
Brooklyn Polytechnic Institute Attn: V. D. Agosta Long Island Graduate Center Route 110 Farmingdale, New York 11735	1
Chemical Propulsion Information Agency Johns Hopkins University/APL Attn: T. W. Christian 8621 Georgia Avenue Silver Spring, Maryland 20910	1
NASA Scientific and Technical Information Facility Attention: Acquisitions Branch P.O. Box 33 College Park, Md. 20740	10
Aerospace Corporation Attn: O. W. Dykema P.O. Box 95085 Los Angeles, California 90045	1
Ohio State University Department of Aeronautical and Astronautical Engineering Attn: R. Edse Columbus, Ohio 43210	1

	Copies
TRW Systems Attn: G. W. Elverum One Space Park Redondo Beach, California 90278	1
Bell Aerospace Company Attn: T. F. Ferger P.O. Box 1 Mail Zone J-81 Buffalo, New York 14205	1
Pratt & Whitney Aircraft Florida Research & Development Center Attn: G. D. Garrison P.O. Box 710 West Palm Beach, Florida 33402	1
Purdue University School of Mechanical Engineering Attn: R. Goulard Lafayette, Indiana 47907	1
Air Force Office of Scientific Research Chief Propulsion Division Attn: Capt. L. R. Lawrence, Jr. (NAE) 1400 Wilson Blvd. Arlington, Virginia 22209	1
Pennsylvania State University Mechanical Engineering Department Attn: G. M. Faeth 207 Mechanical Engineering Bldg. University Park, Pennsylvania 16802	1
University of Illinois Aeronautics/Astronautics Engineering Department Attn: R. A. Strehlow Transportation Bldg., Room 101 Urbana, Illinois 61801	1
NASA Lyndon B. Johnson Space Center Attn: J. G. Thibadaux Houston, Texas 77058	1
Massachusetts Institute of Technology Department of Mechanical Engineering Attn: T. Y. Toong 77 Massachusetts Avenue Cambridge, Massachusetts 02139	1

	Copies
Illinois Institute of Technology Attn: T. P. Torda Room 200 M. H. 3300 S. Federal Street Chicago, Illinois 60616	1
AFRPL Attn: R. R. Weiss Edwards, California 93523	1
U.S. Army Missile Command AMSMI-RKL, Attn: W. W. Wharton Redstone Arsenal, Alabama 35808	1
University of California Aerospace Engineering Department Attn: F. A. Williams P. O. Box 109 LaJolla, California 92037	1
Georgia Institute of Technology Aerospace School Attn: B. T. Zinn Atlanta, Georgia 30332	1
Ultrasystems Attn: T. J. Tyson 2400 Michelson Drive Irvine, California 92664	1
Mr. Donald H. Dahlene U.S. Army Missile Command Research, Development, Engineering and Missile Systems Laboratory Attn: AMSMI-RK Redstone Arsenal, Calabama 35809	1
TISIA Defense Documentation Center Cameron Station Building 5 5010 Duke Street Alexandria, Virginia 22314	1
Office of Assistant Director (Chemical Technology) Office of the Director of Defense Research and Engineering Washington, D.C. 20301	1
D. E. Mock Advanced Research Projects Agency Washington, D.C. 20525	1

	Copies
Dr. H. K. Doetsch Arnold Engineering Development Center Air Force Systems Command Tullahoma, Tennessee 37389	1
Library Air Force Rocket Propulsion Laboratory (RPR) Edwards, California 93523	1
Library Bureau of Naval Weapons Department of the Navy Washington, D.C.	1
Library Director (Code 6180) U.S. Naval Research Laboratory Washington, D.C. 20390	1
APRP (Library) Air Force Aero Propulsion Laboratory Research and Technology Division Air Force Systems Command United States Air Force Wright-Patterson AFB, Ohio 45423	1
Rockwell International Rocketdyne Division Attn: L. P. Combs, D/578 MS BA 17 6633 Canoga Ave. Canoga Park, California 91304	1
Technical Information Department Aeronutronic Division of Philco Ford Corporation Ford Road Newport Beach, California 92663	1
Library-Documents Aerospace Corporation 2400 E. El Segundo Blvd. Los Angeles, California 90045	1
Princeton University James Forrestal Campus Library Attn: D. Harrje Post Office Box 710 Princeton, New Jersey 08540	1
U.S. Naval Weapons Center Attn: T. Inouye, Code 4581 China Lake, California 93555	1

	Copies
Office of Naval Research Navy Department Attn: R. D. Jackel, 473 Washington, D.C. 20360	1
Air Force Aero Propulsion Laboratory Attn: APTC Lt. M. Johnson Wright Patterson AFB, Ohio 45433	1
Naval Underwater Systems Center Energy Conversion Department Attn: Dr. R. S. Lazar, Code TB 131 Newport, Rhode Island 02840	1
NASA Langley Research Center Attn: R. S. Levine, MS 213 Hampton, Virginia 23365	1
Aerojet General Corporation Attn: David A. Fairchild, Mech. Design Post Office Box 15847 (Sect. 9732) Sacramento, California 95809	1
Colorado State University Mechanical Engineering Department Attn: C. E. Mitchell Fort Collins, Colorado 80521	1
University of Wisconsin Mechanical Engineering Department Attn: P. S. Myers 1513 University Avenue Madison, Wisconsin 53706	1
Rockwell International Rocketdyne Division Attn: J. A. Nestlerode, AC46, D/596-121 6633 Canoga Avenue Canoga Park, California 91304	1
University of Michigan Aerospace Engineering Attn: J. A. Nicholls Ann Arbor, Michigan 48104	1
Tulane University Attn: J. C. O'Hara 6823 St. Charles Ave. New Orleans, Louisiana 70118	1

	Copies
University of California Department of Chemical Engineering Attn: A. K. Oppenheim 6161 Etcheverry Hall Berkeley, California 94720	1
Sacramento State College School of Engineering Attn: F. H. Reardon 6000 J. Street Sacramento, California 95819	1
Purdue University School of Mechanical Engineering Attn: B. A. Reese Lafayette, Indiana 47907	1
NASA George C. Marshall Space Flight Center Attn: R. J. Richmond, SNE-ASTN-PP Huntsville, Alabama 35812	1
Jet Propulsion Laboratory California Institute of Technology Attn: J. H. Rupe 4800 Oak Grove Drive Pasadena, California 91103	1
University of California Mechanical Engineering Thermal Systems Attn: Prof. R. Sawyer Berkeley, California 94720	1
ARL (ARC) Attn: K. Scheller Wright Patterson AFB, Ohio 45433	1
Library Bell Aerosystems, Inc. Box 1 Buffalo, New York 14205	1
Report Library, Room 6A Battelle Memorial Institute 505 King Avenue Columbus, Ohio 43201	1
D. Suichu General Electric Company Flight Propulsion Laboratory Dept. Cincinnati, Ohio 45215	1

	Copies
Library Ling-Temco-Vought Corp. P.O. Box 5907 Dallas, Texas 75222	1
Marquardt Corp. 16555 Saticoy Street Box 2013--South Annex Van Nuys, Calif. 91409	1
P. F. Winternitz New York University University Heights New York, N. Y.	1
R. Stiff Propulsion Division Aerojet-General Corp. P.O. Box 15847 Sacramento, California 95803	1
Library, Dept. 596-306 Rockwell International Rocketdyne Division 6633 Canoga Ave. Canoga Park, California 91304	1
Library Stanford Research Institute 333 Ravenswood Ave. Menlo Park, California 94025	1
Library Susquehanna Corp. Atlantic Research Division Shirley Highway and Edsall Rd. Alexandria, Va. 22314	1
STL Techn. Lib. Doc. Acquisitions TRW System Group 1 Space Park Redondo Beach, California 90278	1
Dr. David Altman United Aircraft Corp. United Technology Center P.O. Box 358 Sunnyvale, California 94088	1

	Copies
Library United Aircraft Corp. Pratt & Whitney Division Florida Research and Development Center P.O. Box 2691 W. Palm Beach, Fla. 33402	1
Library Air Force Rocket Propulsion Laboratory (RPM) Edwards, California 93523	1
Kenneth R. Purdy, Professor P.O. Box 5014 Tennessee Technological University Cookeville, Tennessee 38501	1